Journal of Polymer Research (2023) 30:267
https://doi.org/10.1007/s10965-023-03657-y

ORIGINAL PAPER

Mechanical response of the hemp biocarbon-filled hemp-reinforced biopolymer composites

Raj Kumar Dahal[1] · **Bishnu Acharya**[2] · **Animesh Dutta**[1]

Received: 23 February 2023 / Accepted: 15 June 2023 / Published online: 20 June 2023

Abstract

The combined effect of design parameters on the mechanical properties of the biocarbon filled hemp polymer composite offers a newer dimension in biocomposite research. Biopolymer composites with/out hemp fiber and with/out biocarbon fillers were fabricated and optimized. Results showed biocarbon with particle size: 50 microns, filler loading: 10 wt.%, and pyrolysis temperature: 650 °C showed the maximum tensile strength (840.75 MPa with switchgrass biocarbon; 817.02 MPa with hemp biocarbon). Tensile strength of the composite samples was directly proportional to the particle filler loading. Tensile strength initially improved by 50% when particle size increased to 75 µm; a further increase reduced the strength of the composites. The energy at tensile rupture increased with particle size. In contrast, the increased filler loading was detrimental to the energy at break. The parameters positively impacted the samples' flexural strength. Impact strength of the samples fell by 63% when filler loading was doubled to 20 wt.%.

Keywords Hemp composites · Mechanical properties · Biocarbon · Biofillers · Green economy

Introduction

Plant-based materials offer an alternative, environmentally friendly and sustainable pathway towards a greener future. The tailor-made composite materials demonstrate a wide range of materials' properties that individual constituents in the composite material fails to offer. Hemp fibers find their usefulness in thermoplastic and thermosetting polymer composites to produce household products and automotive parts [1] due to their availability, light weight, and performance. These natural fiber-reinforced materials are lightweight and have low density and bids resistance to corrosion, high specific strength, and better stiffness than the forming constituents' fibers and polymers. The low-cost hemp-based materials are easy to process and ecofriendly to use and environment-friendly to disposal [1–6]. Nevertheless, the desired properties of a hemp-based composite material have been found to be dependent upon the type [7–9], orientation [10–16], size [17–21], and properties of the matrix, and the reinforcement. The hemp fibers in composite materials come in different physical properties (aspect ratio), mechanical, thermal, and chemical properties [22–27]. These properties are paramount as the strength and properties of a fiber reinforced composite depends on the alignment and size of these fibers. Because the fibers are aligned in the direction of the load so that the partial load is carried by the fiber that adds the tensile strength and stiffness of the material in the principal stress direction [28–31]. Mechanical strength of hemp fibers has been studied for its superior mechanical properties demonstrated by high tensile strength, tensile modulus and mainly due to its strength-to-weight ratio. Shahzad found out the hemp fiber's tensile strength to be 277 ± 199 MPa, modulus 9.5 ± 5.8 GPa, and failure strain is 2.3 ± 0.8% [32]. Pickering et al. [33] studied the effect of growing period on the hemp fibers' strength. The result showed that the unretted fibres with 114 days of growing period have above 800 MPa tensile strength. Therefore, the fibre's mechanical properties can even be highly affected by the growing time and the selection between retted vs unretted fibres. Additionally, the linearly related stress-strain curves for the hemp fibres shows a huge deviation in the tensile properties

✉ Bishnu Acharya
bishnu.acharya@usask.ca

✉ Animesh Dutta

[1] Bio-Renewable Innovation Lab, School of Engineering, University of Guelph, Guelph N1G 2W1, Canada

[2] Department of Chemical and Biological Engineering, University of Saskatchewan, Guelph S7N 5A9, Canada

among the fibres which is one of the challenges that needs addressing to compare and compete against the synthetic fibres with consistent mechanical properties. On the brighter side, these fibres can still be used as reinforcement to produce strong composite materials wit pre-processing techniques implemented to produce consistent nature fibers. Effect of hemp fibers orientation in the mechanical properties [34, 35] and hemp-epoxy and polymer composites for the mechanical properties [36–39] were investigated for their potential material application. Hence, abundantly available, and short growth period of hemp plants makes them the Suitable resource to design renewable and sustainable materials that supports the fight against global warming and climate change.

On the other hand, fillers in polymer are doped explicitly for the better mechanical, thermal, electrical, and other desired properties. In a study, agricultural wastes such as rice husk, walnut shell, and coconut shell were applied as particulate reinforcement in bio-epoxy resin to investigate the comparative flexural strength in wet and dry conditions. Walnut and coconut showed least water absorption and superior mechanical properties: tensile strength (68.8 MPa), flexural strength (14.9 MPa), and shear strength (81.92 MPa). The elongation at break was 21.82%, energy absorbed during the impact test was 20.9 MPa, and breaking load for tensile and flexural tests of the composite samples with walnut and coconut shells were also better than those of the composites with rice husk and coconut shell fillers and rice husk and walnut shell fillers [40] . Another study involved the plant-based fillers - biocarbon in polyvinyl alcohol in which the fillers were against the materials' tensile strength and storage modulus when measured below the glass transition temperature [41]. This suggests the organic fillers in composite materials can help influence their mechanical as well as physical properties [42].

Various parts of hemp plant find in many useful applications: for instance, the fiber is used as rope, paper, and polymer reinforcement, the leaves are used to extract CBD [43, 44], residual leaves are used as tea [44], hemp seed are good source of nutritional fiber and are added as commodity supplements [45] and to extract hemp oil [46, 47]. However, the hemp stalk does not find any application and is an agricultural waste. This valueless agricultural waste can be turned into a value-added biocarbon filler for polymer composites through pyrolysis. At present, the hemp growers and farmers get rid of the hemp hurd either by leaving it to decompose or by burning it in the field [48]. Moreover, the past research in the mechanical properties of hemp-based materials lacks the investigation of the effect of the biocarbon fillers obtained from hemp. This novel concept of utilization of waste hemp hurd in materials in the form of biofillers will have a significant contribution to the hemp growers, academicians, and scientists.

In this work, hemp stalk and switchgrass feedstock are pyrolyzed at three different temperatures. The obtained biocarbon are added to the hemp fiber-reinforced biopolymer composite system at three different loadings with three different particle sizes. The key mechanical properties of the composite samples are studied and compared.

Materials and method

Biocarbon preparation

We obtained hemp stalk from the Utopia Hemp company, Ontario, Canada, and switchgrass from OBPC Farmers, Ontario, Canada. Hemp fabric was purchased from Effort Industries Inc., Ontario, Canada. Ecopoxy Biopoxy 36 resin with hardener was purchased from Kitchener Fiberglass, Ontario, Canada. We prepared biocarbon through in-house pyrolysis of the hemp stalk and switchgrass feedstock. Hemp stalk and switchgrass were ground and sieved to 200 microns. Biocarbon was obtained by pyrolyzing the hemp and switchgrass feedstock at three different temperatures (450, 550, and 650 °C) in a nitrogen environment. The nitrogen flow was set to 0.75 l/min, the heating rate was kept at 10 °C/min, and the residence time was 30 min. the biocarbon was left to cool under nitrogen conditions inside the reactor.

Biocarbon fillers and composite samples preparation

The obtained biocarbon was crushed and sieved into particle sizes below 50 microns, below 75 microns, and 100 microns. Resin and hardener were taken in the ratio of 4:1 by volume. 6 layers of rectangular hemp fabric (13 cm by 26 cm) were used in each sample. The total weight of the fabric in each sample was 46.6 (± 1.22) g. The biochar filler was added to the resin at 10%, 15% and 20% by resin weight. The resin-hardener-biocarbon mixture was stirred for 2 minutes. A hand layup technique was implemented to prepare the composite samples. The composite was left to cure under a vacuum for 24 hours. The samples were prepared as presented in Table 1 as per the design of experiments.

Physicochemical analyses of the biocarbon

The proximate analysis of the raw samples (hemp stalk and switchgrass) and their biochar samples at various temperatures were performed as per the ASTM standard. The ASTM D3173 was adhered to calculate the moisture in the samples. D3175-20 was followed to analyze the samples' volatile matter, and ASTM E1755-01(2020) adhered to find the ash in the samples. The fixed carbon was calculated from the difference.

Table 1 The Samples and their compositions.

Sample Code	Composites	Biocarbon	Reinforcement	Pyrolysis Temperature (°C)	Particle Size (μm)	Filler Loading (wt. %)
a)	H45-50-10	Hemp	Hemp	450	50	10
b)	H45-50-20	Hemp	Hemp	450	50	20
c)	H45-100-10	Hemp	Hemp	450	100	10
d)	H45-100-20	Hemp	Hemp	450	100	20
e)	H55-75	Hemp	Hemp	550	75	15
f)	H65-50-10	Hemp	Hemp	650	50	10
g)	H65-50-20	Hemp	Hemp	650	50	20
h)	H65-100-10	Hemp	Hemp	650	100	10
i)	H65-100-20	Hemp	Hemp	650	100	20
k)	S45-50-10	Switchgrass	Hemp	450	50	10
l)	S45-50-20	Switchgrass	Hemp	450	50	20
m)	S45-100-10	Switchgrass	Hemp	450	100	10
n)	S45-100-20	Switchgrass	Hemp	450	100	20
o)	S55-75	Switchgrass	Hemp	550	75	15
p)	S65-50-10	Switchgrass	Hemp	650	50	10
q)	S65-50-20	Switchgrass	Hemp	650	50	20
r)	S65-100-10	Switchgrass	Hemp	650	100	10
s)	S65-100-20	Switchgrass	Hemp	650	100	20
j)	HeR	None	Hemp	None	None	None
t)	HaR	None	None	None	None	None

Flash 2000 Organic elemental Analyzer CHNS-O Analyzer performed the samples' ultimate analysis. The instrument determined carbon, oxygen, nitrogen, and sulphur. Oxygen content was determined from the difference by subtracting the C, H, N, S, and ash content from the total.

X-ray photoelectron spectroscopy (XPS)

A Kratos (Manchester, UK) AXIS Supra system at the Saskatchewan Structural Sciences Centre (SSSC)was used to collect the X-ray Photoelectron Spectroscopy (XPS) images. A spot size of hybrid slot (300×700) microns was used. The spectra were scanned in the 0–1200 eV binding energy range in 1 eV steps with a pass energy of 160 eV. The obtained XPS spectra were analysed and deconvoluted using the Gaussian–Lorentzian sum function. Atomic ratios mainly of C, O, Si, and Ca were involved in the peak C(1s), Ca(2p), Si(2p), and O(1s), respectively. In this study, the elemental composition was applied to compare the biocarbon samples at different temperatures and to compare their effect on the composites' properties; absolute chemical composition was not studied.

Tensile test

The Instron 5969 was used to study the tensile behaviour of the prepared composite samples as per the ASTM standard D3039. Each sample of 100 mm length was tested. From this test, the load (N) against the extension (mm) up to the point of breakage was recorded. Then the curves were transformed into stress–strain curves. Each composites type had two replicates. Five test coupons were cut out from each sample to perform the tensile test.

Flexural test

Three-point bending (flexural test) was performed with Instron 5965 with 5 kN cell as per the ASTM D790-17 (Standard test method for flexural properties of unreinforced and reinforced plastics and electric insulating materials). The samples were sized as per the standard and the tests were repeated for accuracy. The rate of the load was taken as per the following formula:

$$R = Z \times L^2/6D$$

where:
R = crosshead speed (mm/min)
Z = 0.01
L = distance between the supports = 50 mm
D = Depth of the sample (mm)
Hence, R = 4.2/D

Impact test

Results from the impact test was provided by department of chemical engineering, University of Saskatchewan for the impact test. ASTM D256 – 10 (2018): Standard test methods for determining the Izod pendulum impact resistance of plastics were used to determine the impact energy of the samples. DH-1843-5.5D Izod impact tester was used to determine the impact energy. The impact energy was set to 15 J at 3.5 m/s. The tests were repeated for a minimum of four runs to obtain accurate results.

Hardness test

Brinell hardness test was on a United Tru-Blue Universal machine (USA) following the ASTM E10-18 Standard. Carbide ball indenter of 2.5 mm diameter was used to apply a load of 62.5 kgf; the load was held for 10 seconds. The tests were repeated for a minimum of six runs (two tests in three different rows) to obtain the accurate results. The measured hardness was recorded in HBW 2.5/62.5/10; 2.5 indicating the indenter ball diameter, 62.5 being the applied load in kgf for 10 seconds.

SEM analysis

The surface morphology of the composites was studied under the FEI Quanta 250 Field Emission Scanning Electron Microscope (FE-SEM) by generating magnified cross-sectional views on the tested tensile samples. The accelerating voltage was set to 20 kV, and a working distance of 10 mm was maintained. The instrument was set to 4.19 x 10-6 bar vacuum pressure. The samples obtained from the tensile tests were fractured in normal room conditions by shearing with a bolt cutter. Before their microscopic imaging, each sample was sputter-coated under Helium in a Desk V Denton Vacuum instrument.

Data analysis

The data from the thermal tests were statistically analyzed with a confidence level of 95% for all the composites (p-value 0.05). The average values with standard deviations were reported. One-way analysis of variance (ANOVA) was performed using Design Expert statistical software, and optimization was performed.

Results and discussion

Biocarbon physiochemical properties

Figure 1a shows the volatile matter comparison of the biocarbons obtained from the hemp stalk and switchgrass pyrolysis. It is shown that the pyrolysis temperature is indirectly proportional to the volatile matter of the resulting biocarbon samples. Figure 1a also shows that the hemp biocarbons contain slightly higher volatile matter compared to the switchgrass biocarbon samples measured at the same temperatures.

It can be observed that as the pyrolysis temperature increases from 450 °C to 650 °C, the percentage of volatile matter decreases for both the Hemp stalk and Switchgrass samples. This indicates that the higher temperature leads to more complete pyrolysis, resulting in a lower percentage of volatile matter. Figure 1b further illustrates a negligible difference in the biocarbon samples' H:C ratio obtained from two different feedstocks at three different pyrolysis temperatures: 450 °C, 550 °C, and 650 °C. The Figure further explains the decreasing trend of the ratio with the increase in pyrolysis temperature due to the increase in carbon content and subsequent elimination of the hydrogen present in the samples during the higher temperature pyrolysis.

The O/C ratio in Fig. 1c shows a similar trend shown by the H/C ratio. Here the decline in the ratio is aggressive with the increase in pyrolysis temperature as the abundantly available oxygen in biomass gets eliminated drastically in the subsequent higher pyrolysis temperatures. In addition to that, the O/C ratios of switchgrass biocarbon samples were observed higher compared to the hemp biocarbon samples.

X-ray photoelectron spectroscopy (XPS)

The surface chemistry of the biocarbon was performed with the help of XPS spectroscopy. The obtained spectra are illustrated in Figs. 2, 3, 4, 5. With XPS, the elemental composition of the sample, as well as its atomic and mass concentrations, was determined. These measurements are useful for understanding surface chemistry. Based on the high-resolution XPS spectrum of C1s for the biocarbon samples, the deconvolution procedure identified the energy range 283-284.45 eV which is associated to the 1s-π transition causing the C=O bond in quinine C with G1 deconvolution curve. Similarly, at the energy range of 284-285.5 eV is due to the 1s-π transition causing the C=C with aromatic C, C=H in protonated and alkylated aromatic C, and carbonyl substituted aryl C in G2 deconvolution curve [49–57]. Notably, Calcium (Ca 2p) at 347 eV energy separates the biocarbon obtained from the hemp stalk at 650 °C from the rest of the biocarbon samples. Other identified peaks with descending concentrations were Oxygen (O1s) at 531 eV and Silicon (Si 2p) at 101 eV. The presence of calcium in the biochar will have an influence in the mechanical behaviour of the polymer composites [58].

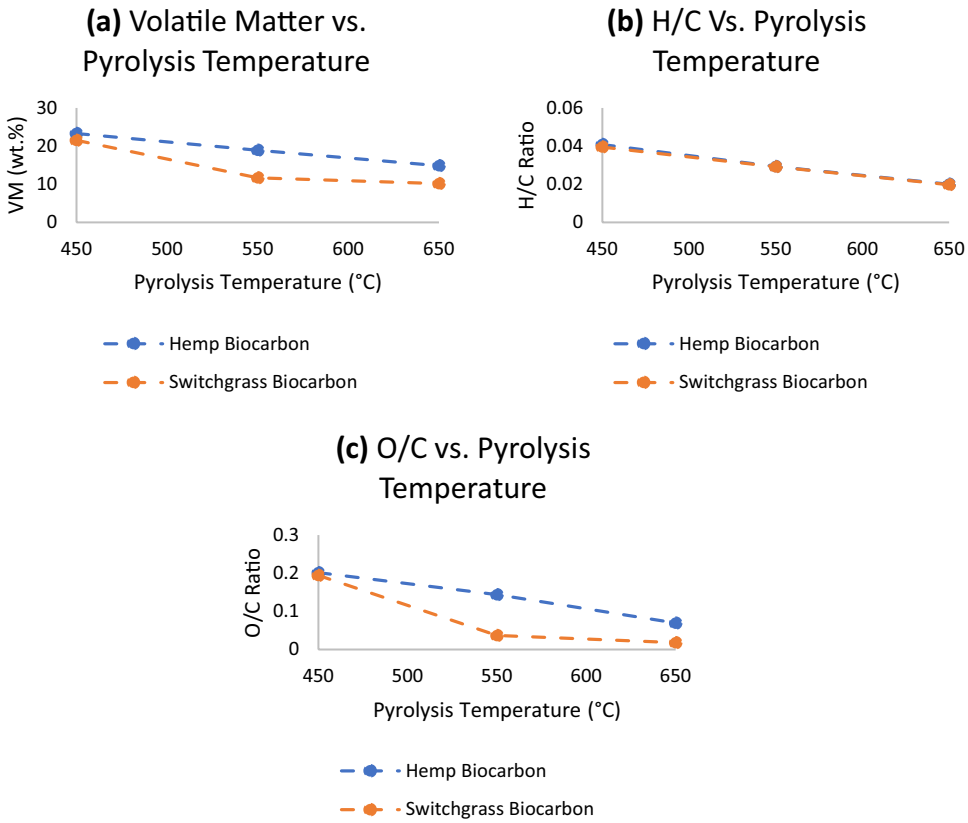

Fig. 1 **a** change in the volatile matter, **b** H/C ratio, and **c** O/C ratio with the pyrolysis temperature to prepare the biocarbon samples

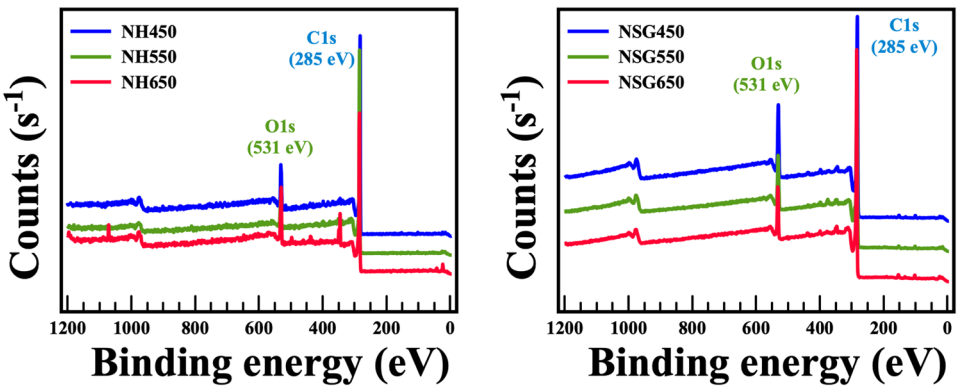

Fig. 2 General XPS spectra for the biocarbons from the hemp stalk and switchgrass at 3 different temperatures

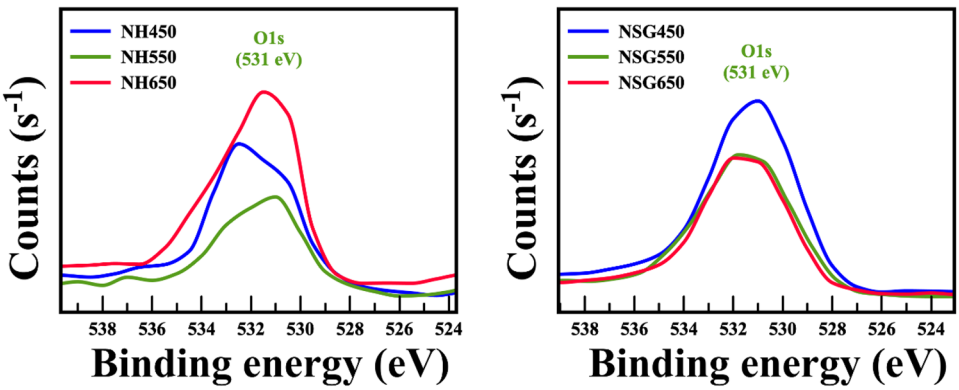

Fig. 3 XPS spectra of the peak deconvolution for O1s (Oxygen) for the biocarbons from the hemp stalk and switchgrass at 3 different temperatures

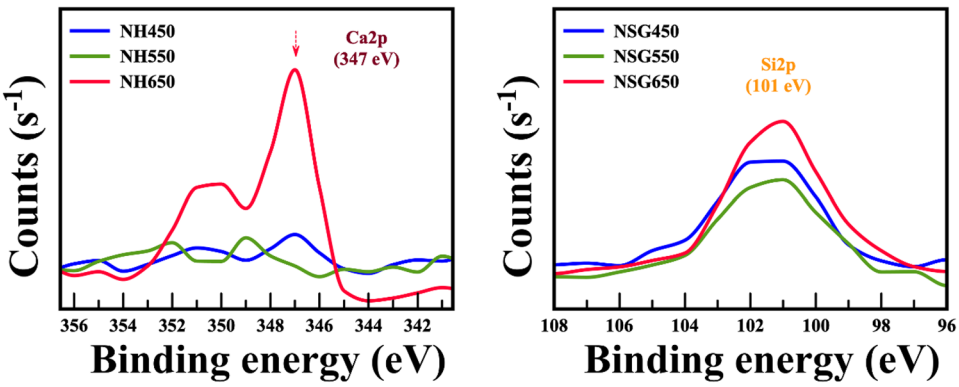

Fig. 4 XPS spectra of the peak deconvolution for Ca2p (Calcium) for the hemp biocarbon at 650 C, and Si2p for the switchgrass biocarbons at 3 different temperatures

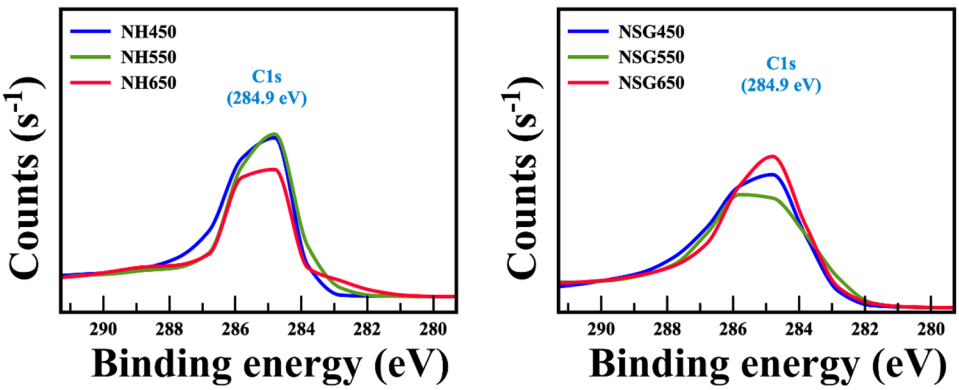

Fig. 5 XPS spectra of the peak deconvolution for C1s (Carbon) for the biocarbons from the hemp stalk and switchgrass at 3 different temperatures

Tensile strength of the hemp fiber-reinforced composites

The composite samples showed a change in mechanical strength with the change in biocarbon filler type and properties. The findings from the tensile test on the hemp fiber reinforced polymer composites are provided in Table 2.

Figures 6, 7, and 8 summarize the main effects of the design factors (pyrolysis temperature, particle size and filler loading) on the resultant composite samples' tensile strength.

The pyrolysis temperature of the biocarbon influenced the tensile strength of the resulting composite samples. The tensile strength of the biocarbon-filled hemp reinforced

Table 2 The mean tensile properties of biocarbon-filled hemp fiber-reinforced biopolymer composites.

				Hemp Biocarbon-Filled Composites		Switchgrass Biocarbon-Filled Composites	
Sample Code	Pyrolysis Temperature (°C)	Particle Size (μm)	Filler Loading (wt.%)	Tensile Strength (MPa)	Energy at Break (J)	Tensile Strength (MPa)	Energy at Break (J)
45-50-10	450	50	10	802.02 (±17.26)	2.91 (±0.14)	748.08 (±195.06)	3.00 (±0.34)
45-100-10	450	100	10	713.00 (±35.75)	2.37 (±0.65)	748.11 (±82.05)	2.48 (±0.41)
45-50-20	450	50	20	678.36 (±57.75)	3.92 (±0.20)	635.60 (±94.27)	4.93 (±0.65)
45-100-20	450	100	20	649.24 (±2.68)	2.63 (±.50)	530.62 (±119.97)	2.70 (±1.12)
55-75	550	75	15	778.38 (±101.30)	3.40 (±0.90)	755.82 (±61.09)	3.27 (±1.35)
65-50-10	650	50	10	817.02 (±114.94)	3.73 (±1.17)	840.75 (±27.05)	3.16 (±1.38)
65-100-10	650	100	10	723.33 (±6.97)	2.88 (±0.62)	833.69 (±91.48)	2.20 (±0.75)
65-50-20	650	50	20	713.16 (±4.53)	4.47 (±0.57)	701.18 (±94.88)	2.92 (±1.25)
65-100-20	650	100	20	646.13 (±127.57)	3.21 (±0.76)	553.64 (±13.56)	2.50 (±0.87)

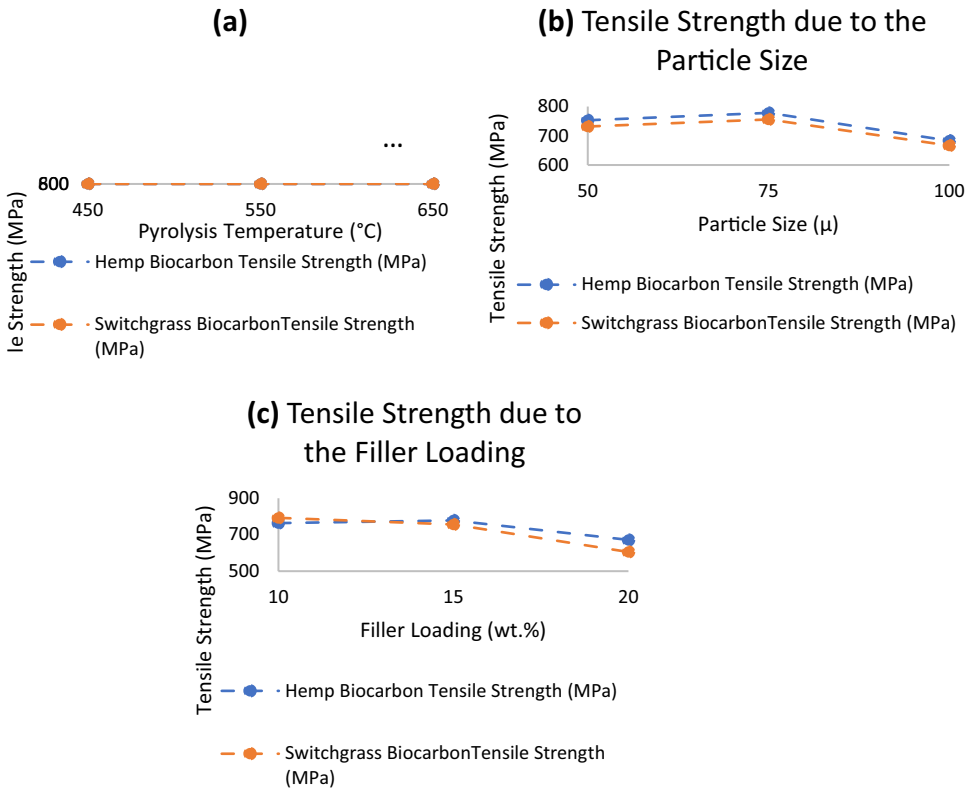

Fig. 6 The effect due to **a** pyrolysis temperature, **b** particle size, **c** filler loading on the mean tensile strength of the hemp fiber-reinforced composite samples

polymer composites increased when the pyrolysis temperature of the biocarbon increased from 450 °C to 550 °C; however, the strength decreased when the temperature was further raised to 650 °C as shown in Fig. 6a, irrespective of the filler type. The observed trend in the tensile strength of the biocarbon-filled hemp reinforced polymer composites with increasing pyrolysis temperature can be attributed to the change in the properties of the biocarbon filler material.

The biocarbon at a lower temperature (450 °C) contains more volatile matter and have a lower degree of carbonization, which can result in a filler material with lower strength and stiffness. As the pyrolysis temperature increases to 550 °C, the biocarbon becomes more carbonized and less porous, leading to an increase in its strength and stiffness. However, when the temperature is further increased to 650 °C, the biocarbon may become excessively carbonized and brittle, resulting in a decrease in its strength.

Also, the observed trend could be the effect of the filler morphology on the composite properties. More irregular shape and surface of the biocarbon at lower pyrolysis

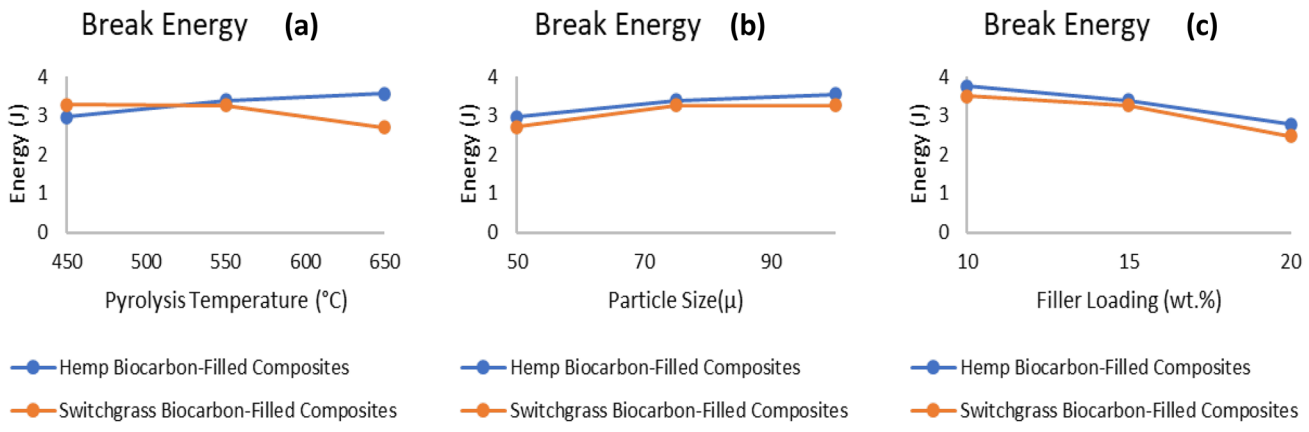

Fig. 7 The influence of the **a** pyrolysis temperature, **b** particle size, and **c** filler loading on the breaking energy of the hemp fiber-reinforced biocarbon-filled polymer composite samples

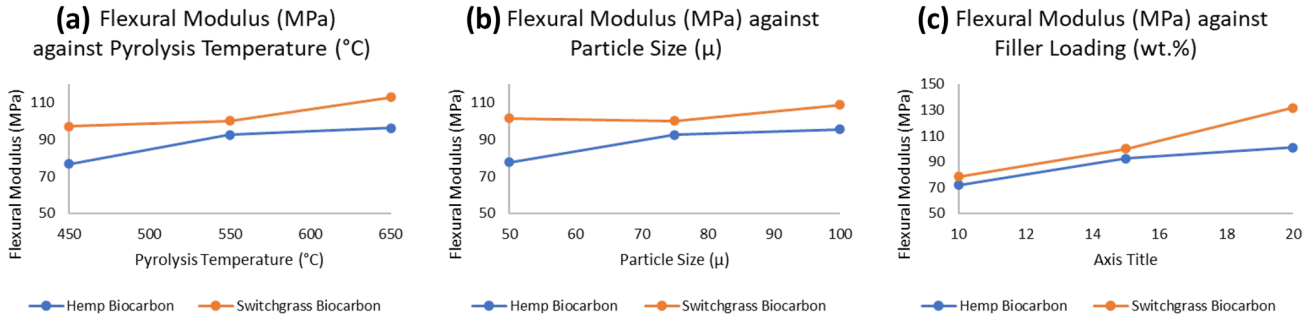

Fig. 8 The change in flexural modulus of the biocarbon-filled hemp fiber-reinforced biopolymer composites due to **a** pyrolysis temperature, **b** particle size, and **c** filler loading

temperature can lead to weaker interfacial bonding between the biocarbon and polymer matrix. As the pyrolysis temperature increases, the biocarbon particles may become more uniform and have smoother surfaces, resulting in better interfacial bonding and higher composite strength. However, at higher temperatures, the biocarbon particles may start to agglomerate losing their shape, resulting in weaker interfacial bonding and lower composite strength.

The maximum value of tensile strength was 840.75 MPa for S65-50-10 and 817.02 MPa for H65-50-10. These values are higher than the strength of the unfilled and unreinforced polymer composite (HaR) by about 200% and 208% respectively, and these strengths are higher from the unfilled composites reinforced with hemp fiber by 12.27% and 2.80% respectively. This shows that both filler types have enhanced the rigidity of the biopolymer composite samples. Similar results with improved mechanical properties by adding natural plants-based fillers were claimed in the past research [59–62]. The unfilled and unreinforced polymer composite experiences brittle failure when tensile load is applied. This failure is further supported by the voids and microcracks present in the polymer matrix. This is why the unreinforced and unfilled polymer composites showed the poor tensile properties. The tensile properties show a great improvement by introducing the fiber into the system. The presence of hemp fiber-polymer matrix interlocking interface helps transfer stress to avoid the formation of macro cracks from micro cracks up to a critical load at which the cracks promote material failure. Thus, stress transfer depends upon the bonding between the polymer matrix and the hemp fiber properties. A weaker matrix-reinforcement results in earlier fiber pullouts and weaker tensile strength, while a strongly bonded interface results in fiber cracking. This bonding between the matrix and the fibers is contributed by the adhesive force of the polymer matrix, shear force between the interlocked interfaces, and the frictional force between the hemp fibers and the polymer interfacial surface. Therefore, the introduction of the biocarbon in the polymer matrix has increased the frictional force between the fiber and the polymer matrix that has initially increased the tensile strength of the composite material. Further addition of the filler particles, although increased the frictional force, reduced the adhesive force between the polymer matrix and the hemp fibers. Therefore, the tensile strength decreased significantly while adding the biocarbon fillers to 20 wt.%. The lowest tensile strength was observed in the samples with 20% filler loading of the 100 microns particle sized biocarbon fillers obtained at 650 °C, irrespective of the feedstock type. The tensile strength at this condition was 646.13 MPa and 553.64 MPa for hemp biocarbon and switchgrass biocarbon, respectively.

As shown in Fig. 6b, an initial rise in tensile strength was observed when the fillers' particle size was increased from 50 μm to 75 μm. Then the strength of the samples decreased on further increasing the particle size to 100 μm. This effect was observed in both biocarbon filler types. The improved tensile strength can be associated with an effective stress transfer in the composite samples with 75 μm particle sized fillers when the tensile load was applied. Further increase in particle size weakened the fiber-matrix bond resulting in weaker tensile strength. The weaker bond causing debonding of the fibers can also be caused due to the agglomeration and uneven distribution of the bigger sized fillers in the polymer matrix. The initial increase in the friction force between the polymer matrix and the hemp fiber as well as the adhesive force of the polymer matrix to hold the hemp fiber has led the tensile strength to rise. Further increment of the particle size weakened the adhesive force of the polymer matrix to hold the hemp fibers.

Figure 6c shows that the composite samples' tensile strength decreased when the filler content was increased, regardless of the filler type. At 15 wt.% filler loading there is a non-significant change in tensile strength compared with the samples with 10% filler loading. This decline in the tensile strength can be attributed to the poorer matrix-filler-fiber interfacial bonding when the filler content was increased. This weaker interfacial bonding results in easier debonding of the fibers from the matrix and results in a

poorer stress transfer mechanism when the tensile load is applied. Moreover, the unevenly distributed biocarbon forms agglomeration in the matrix that compromises with the resulting tensile properties of the composite samples. Both, there was a similar trend in change of the tensile strength in the biocomposite samples with hemp biocarbon and switchgrass biocarbon fillers. As the matrix-filler adhesion plays a vital role to determine its resulting mechanical properties [59, 63], the decrease in the tensile strength with increased particle size and the filler loadings in the composites may also be attributed to the loss of the adhesion of the larger filler particles to the polymer matrix. The authors have suggested that the loss in adhesion may be due to the increased surface area of the filler, poor wettability of the highly loaded filler in the composites and an easy debonding of the filler- polymer interface [59].

These findings further boost the previous conclusions of the dependence of the tensile strength of the composite samples on the compatibility of the filler into the polymer matrices' microstructure. A stronger composite material can be achieved by optimizing the amount, size, and type of biocarbon filler.

Energy at break of the hemp fiber-reinforced composites

The fracture toughness of a material can be studied by determining the energy required to break it. Table 2 summarizes the energy at break and hence the fracture toughness of the hemp fiber-reinforced biocarbon-filled polymer composites. The increased pyrolysis temperature had a positive impact on the hemp biocarbon-filled composites whereas the energy at the break decreased by increasing the switchgrass biocarbon's pyrolysis temperature. The energy at the break of a composite material (fracture energy) represents the work done per unit area to fracture the material during the tensile load. The energy at the break of the hemp-reinforced composite samples is presented in Fig. 7.

The tensile test of the composite samples showed that the energy required to break the samples is influenced by the particle size and loading of the biocarbon fillers. The energy at break was found to increase by increasing the particle size from 50 to 100 microns whereas the effect was reversed when higher amount of biocarbon filler was added into the composite samples. These effects were consistent in both types of biocarbons obtained from hemp stalk and switchgrass pyrolysis. The pyrolysis temperature increased the breaking energy of the composite samples with the hemp biocarbon was used and the value depleted by switching into the switchgrass biocarbon. This difference in the breaking energy can be explained with the XPS images shown in Fig. 8 which shows the binding energy of the hemp composite at higher temperature (650 °C) going off the trend due to the presence of calcium in the biocarbon sample. The depiction of calcium at higher temperature is due to its increased concentration in the ash at higher temperature in the biocarbon as observed through the proximate analysis. The higher breaking energy suggests the stronger energy required to rupture the matrix-fiber bond. This can be inferred as the bonding of the biocarbon-polymer and fiber gets stronger by increasing the particle size from 50 to 100 microns and the bond weakens as the filler loading is increased from 10 to 20 wt.%. Finally, the test showed that the rupture energy per area of the unfilled hemp fiber-reinforced polymer composite was 162.03 ± 34.36 kJ/m2, which was seen to be the highest among all composite samples. This result suggests that the biocarbon in hemp-fiber reinforced composite samples degrades its energy at break during the tension force.

Flexural properties of the hemp composites

Results from the three-point bend test for the flexural strength analysis of the hemp-reinforced composites are presented in Figs. 8 and 9. The findings have been summarized in Table 3. Figure 8 illustrates the main effect of the design parameters (pyrolysis temperature, particle size, and filler loading) on the flexural modulus of the resulting composite samples.

The pyrolysis temperature increase in both filler types (hemp biocarbon and switchgrass biocarbon) increased the flexural modulus of the composite materials. This effect is due to the better absorption of the resin inside the larger pores of the filler biocarbon obtained at higher temperatures resulting in a stronger matrix-reinforcement interface. Similarly, the particle size and filler amount had a positive effect on the flexural strength of the composite samples. The results show a minimum flexural modulus (42.73 MPa) of unreinforced unfilled polymer composite due to its brittle nature in absence of fiber and filler. The hemp fiber raised this value by 39% to 59.5 MPa. This is because more fibers are present in the area where it would crack otherwise due to flexural loading.

The results from the flexural test also showed that the design parameters affect the breaking flexural load as shown in Fig. 9. The pyrolysis temperature first increases the breaking stresses when it is raised from 450 °C to 550 °C. A further increase in the pyrolysis temperature was seen to reduce the breaking load of the composite samples. Similar effect was observed while the particle size and the filler loading were increased. The composite samples with 15 wt.% 75 microns sized of biocarbon obtained at 550 °C showed the greatest breaking stress among all composite samples. The increased flexural properties are again due to the improved friction between the matrix-reinforcement due to the addition of the fillers in the system. The inclusion of the fillers in the polymer matrix has delayed the crack propagation

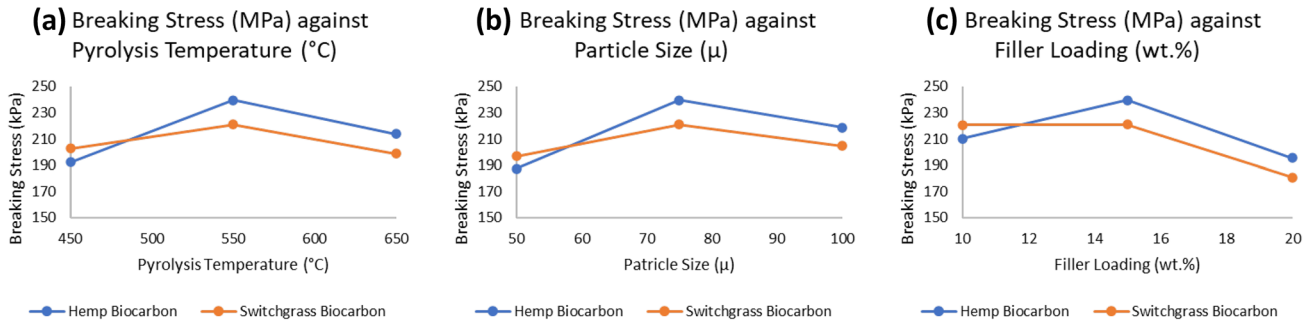

Fig. 9 The change in breaking stress (Breaking load per unit area) of the biocarbon-filled hemp fiber-reinforced biopolymer composites during the flexural loading due to **a** pyrolysis temperature, **b** particle size, and **c** filler loading

thus improving the flexural modulus. Moreover, the flexural strength is higher with the longer fibers are they offer larger bonding surface with the matrix thus increasing the fiber-pull-out load [64, 65].

The composite samples without biocarbon fillers showed the breaking stress of 225.96 ±41.35 kPa, the flexural strength of 4.10 ± 0.09 MPa, and the flexural modulus of 56.02 ± 6.10 MPa. This shows that the biocarbon fillers in composite samples significantly increase their flexural modulus.

Impact test

The obtained impact energy to break the sample was divided by the thickness to obtain the impact strength of the composite samples as per the ASTM standards. Table 4 summarizes the findings from the impact test of the hemp fiber-reinforced polymer composite samples.

As shown in Table 4, the composite samples' impact energy was greatly influenced by the design parameters (pyrolysis temperature, biocarbon fillers' particle size, and biocarbon filler loading). The main effects of the individual parameters are demonstrated in Fig. 10.

Impact energy refers to the energy dissipated during the impact loading on the composite material during which the fiber pullouts, fractures, matrix deformation, matrix rupture, and material failure takes place. The impact energy of the hemp fiber reinforced composites without biocarbon fillers showed a value of 8.09 ± 2.22 J/m (when measured as per the ASTM standard) and 630.31 J/m2 (as per the ISO standard). These values of impact energies are significantly higher than those of the biocarbon filled composite samples. This can be inferred as the biocarbon in the composite samples promotes earlier material failure during the impact loading. Similarly, the gradual increment of the pyrolysis temperature of the obtained biocarbon decreased the impact strength of the composite materials up to 550 °C and further increase in the temperature had positive effect on the impact strength of the material samples. Furthermore, the particle size showed a very similar effect to that of the pyrolysis temperature. The filler loading had a negative effect on the impact strength of the measured composite samples. The value of the impact strength decreased by almost 63% when filler loading was increased to 20 wt.%.

Table 3 The summary Table showing the flexural properties of the hemp-reinforced polymer composites

Sample Code	Pyrolysis Temperature (°C)	Particle Size (μm)	Filler Loading (wt.%)	Hemp Biocarbon-Filled Composites			Switchgrass Biocarbon-Filled Composites		
				Flexural Modulus (MPa)	Flexural Break Stress (kPa)	Max. Flexural Stress at Break (MPa)	Flexural Modulus (MPa)	Flexural Break Stress (kPa)	Max. Flexural Stress at Break (MPa)
45-50-10	450	50	10	68.90	176.50	4.27	76.63	176.77	4.57
45-50-20	450	50	20	81.65	166.20	4.14	120.59	180.82	4.66
45-100-10	450	100	10	61.02	218.16	3.96	72.01	263.20	4.08
45-100-20	450	100	20	95.83	207.69	4.39	119.79	190.58	4.96
55-75	550	75	15	92.51	239.51	4.42	100.18	220.91	4.62
65-50-10	650	50	10	70.57	210.79	4.16	63.22	248.38	4.07
65-50-20	650	50	20	89.52	195.66	4.78	145.37	181.52	4.71
65-100-10	650	100	10	87.85	235.54	4.35	101.70	194.51	4.75
65-100-20	650	100	20	137.25	212.97	4.87	141.92	170.84	5.06

Table 4 The summary Table showing results from the impact test pf the hemp fiber-reinforced composite samples

Sample Code	Pyrolysis Temperature (°C)	Particle Size (μm)	Filler Loading (wt.%)	Hemp Biocarbon-Filled Composites		Switchgrass Biocarbon-Filled Composites	
				Average Impact Strength (J/m)	Average Impact Strength (J/m2)	Average Impact Strength (J/m)	Average Impact Strength (J/m2)
45-50-10	450	50	10	1.58 (±0.10)	123.00 (±9.18)	1.29 (±0.13)	101.39 (±9.65)
45-50-20	450	50	10	0.69 (±0.13)	53.46 (±9.76)	0.54 (±0.12)	41.58 (±8.76)
45-100-10	450	100	10	1.73 (±0.24)	132.01 (±18.74)	1.51 (±0.36)	114.25 (±27.32)
45-100-20	450	100	20	0.54 (±0.13)	40.80 (±9.97)	0.67 (±0.15)	50.50 (±11.43)
55-75	550	75	15	0.45 (±0.04)	34.28 (±3.54)	0.60 (±0.08)	45.92 (±5.31)
65-50-10	650	50	10	1.47 (±0.08)	110.64 (±5.27)	1.87 (±0.40)	141.15 (±29.36)
65-50-20	650	50	20	0.61 (±0.00)	46.23 (±0.44)	0.56 (±0.05)	42.43 (±3.07)
65-100-10	650	100	10	1.28 (±0.15)	98.67 (±11.17)	1.50 (±0.08)	115.05 (±5.22)
65-100-20	650	100	20	0.59 (±0.09)	44.15 (±6.72)	0.73 (±0.13)	55.12 (±10.09)

Hardness test

The influence of pyrolysis temperature, the filler size and the filler loading on the hardness of the hemp reinforced bioepoxy composites is presented in Table 5. The samples show the effect on their hardness (tested with the Brinell Hardness test) with varying biocarbon temperature, its particle size, and its loading.

Test results showed that the hemp fiber in the polymer matrix increased its hardness by 51.19% to 31.75 HBW. The integration of 10 wt.% biocarbon filler in the hemp fiber-reinforced polymer, as shown in the comparative Fig. 11, first decreased the hardness of the polymer composite regardless of the filler type. Further increasing of the filler content to 20% increased the hardness of the composite materials from the 10% filled biocomposites in both

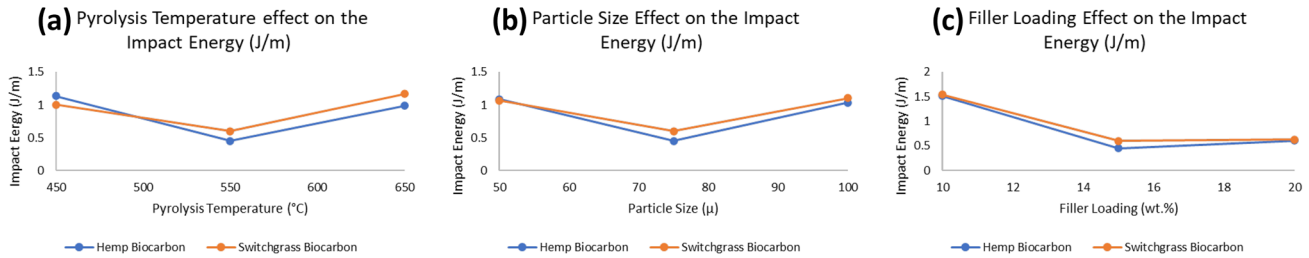

Fig. 10 The impact energy of the composite samples due to **a** pyrolysis temperature, **b** particle size, and **c** filler loading

Table 5 The measured values of the hardness (in HBW) of various hemp fiber-reinforced composite samples with biocarbon fillers

Sample Code	Pyrolysis Temperature (°C)	Particle Size (μm)	Filler Loading (wt.%)	Hemp Biocarbon Composite Hardness (HBW)	Switchgrass Biocarbon Composite Hardness (HBW)
45-50-10	450	50	10	26.57 (±1.29)	29.5 (±2.64)
45-50-20	450	50	20	32.45 (±2.59)	33.25 (±2.46)
45-100-10	450	100	10	22.14 (±2.08)	26.14 (±1.60)
45-100-20	450	100	20	23.43 (±0.55)	27.33 (±1.25)
55-75	550	75	15	26.67 (±0.89)	29.83 (±1.62)
65-50-10	650	50	10	29.25 (±1.86)	30.14 (±0.50)
65-50-20	650	50	20	32.17 (±2.07)	34.8 (±3.27)
65-100-10	650	100	10	25.43 (±1.46)	27.13 (±1.62)
65-100-20	650	100	20	28.75 (±1.51)	29.67 (±0.96)

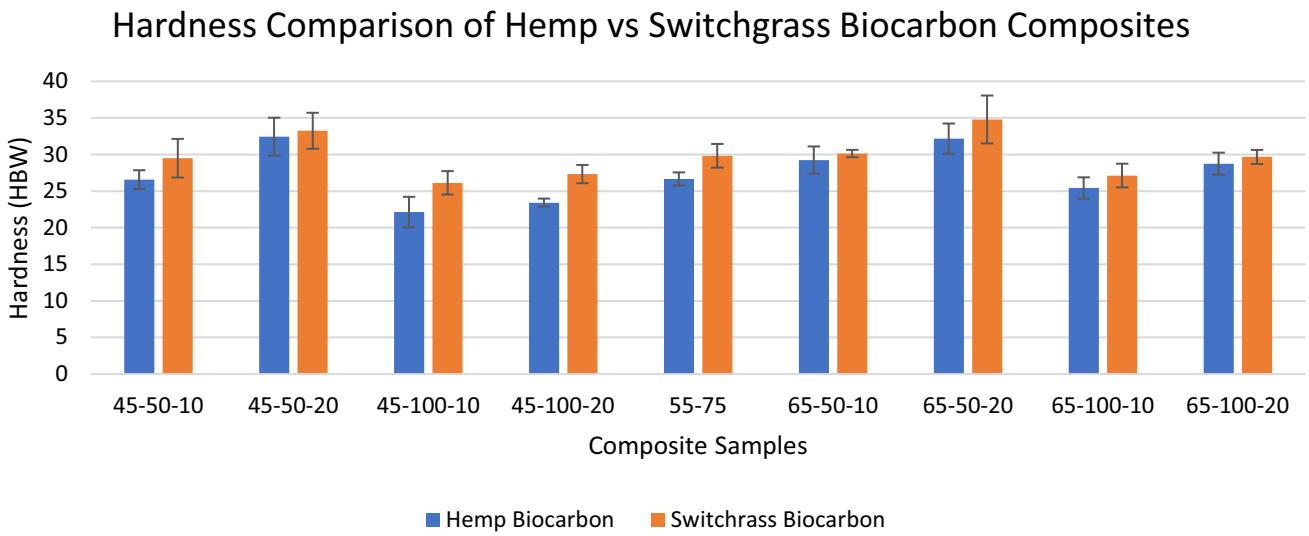

Fig. 11 The comparative study of the mean hardness of the biocarbon-filled hemp fiber-reinforced biopolymer composites

types of biocarbon filled samples. However, the increased value was still lower than the maximum hardness of the composites that was seen in the unfilled hemp composites. The hemp biocarbon filled composites experienced the least hardness. The hardness of the composites significantly increases with the increase in filler loading from 10 wt.% to 20 wt.%. This has been attributed to the filler properties that enhance the mechanical properties of the resin-hardener composites. The incorporation of the fillers in the composite systems inherits its hardness properties to the composite system. The increased hardness also signifies the stronger interfacial interactions between the filler particles and the polymer in the composite samples. It can also be seen that the hemp biocarbon-filled composites have comparatively lower hardness values compared to their counterpart switchgrass biocarbon-filled composites. This could be attributed to the carbon content of the filler as shown in Table 2.

The main effects of the individual factors (pyrolysis temperature, particle size, and filler loading) on the hardness of the resulting hemp fiber-reinforced polymer composites are shown in Fig. 12.

As shown in Fig. 12a, the hardness of the biocarbon-filled composites has experienced an increase in value with the increase in the pyrolysis temperature from 450 °C to 650 °C. This can be attributed to the change in carbon content, oxygen level and the hydrogen in the biocarbon with the changed temperature leaving behind more porous carbonaceous material. The change in H/C ratio and O/C ratio is presented in Fig. 1. Similarly, the hardest composite was

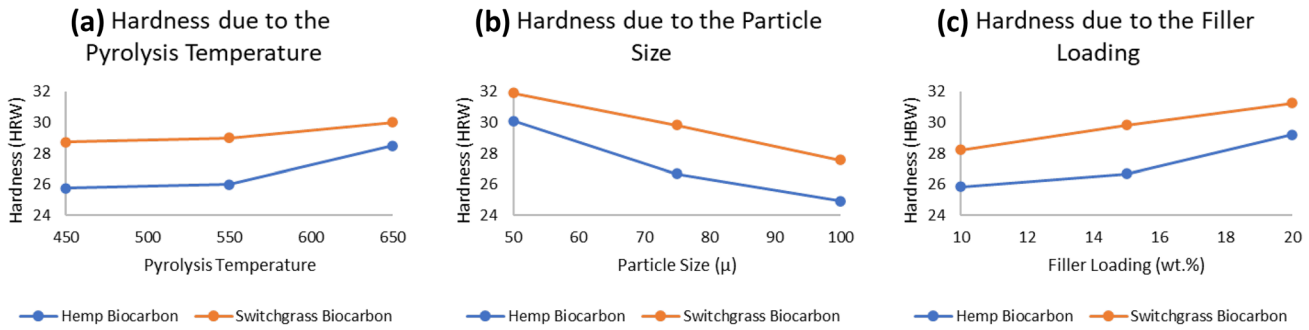

Fig. 12 The effect of **a** pyrolysis temperature, **b** particle size, and **c** biocarbon filler loading in the samples' mean hardness

obtained when small sized filler particles were added in the composite material as depicted in Fig. 12b. The ability to distribute evenly in the epoxy resin of the smaller particle sizes results in a more homogeneous mixture which forms a stronger bond with the fiber reinforcement. The larger particle sizes may result in voids and space that may have compromised with the hardness of the composite material as shown by the SEM images.

Figure 13c suggests that the hardness of the composite materials significantly increased with the increase in filler loading. The harder biocarbon filler has contributed its properties towards the increased hardness of the resulting material with higher filler concentration. These effects were almost identical in both types of feedstocks (i.e., hemp biocarbon and switchgrass biocarbon fillers). The measured hardness of the resin-hardener composite was found to be 21 HBW which is the least among all composite samples. Hence the biocarbon in bioepoxy matrix enhances its stiffness and the resistance to the plastic deformation when the load is applied to it [66]. Also, the hardness of the composites is highly dependent on the filler properties including its surface area, porosity, hardness, and its bonding compatibility with the polymer [59, 60].

Failure mechanism

Figures 13 and 14 shows the damaged samples during the tensile and flexural tests, respectively. The failure in tensile test was due to the breaking of both fibers and cracking of the polymer matrix. While the failure during the three-point bending analysis was due to mainly polymer failure. The load is redistributed among the remaining fibers through the matrix when one fiber starts breaking off. A cross-ply composite subjected to the tensile loading fails due to several subsequent damage modes: the first one being the matrix cracking (known as first ply failure) in the transversa lamina. This is because of the weaker nature of the polymeric matrix as compared to the longitudinally loaded hemp fibers. This causes in the drop of the transverse tensile modulus of the composite material. The lateral splitting of the fibers with further tensile load is the second ply failure. The fiber fracture takes place in further increasing the tensile loading [67].

Similarly, Fig. 14 shows the failure in composite samples visible on the compression side. During the test and observations, it was seen that the delamination only occurred near the fractured surface. This was followed by the fiber breakage on further increment of the flexural loading.

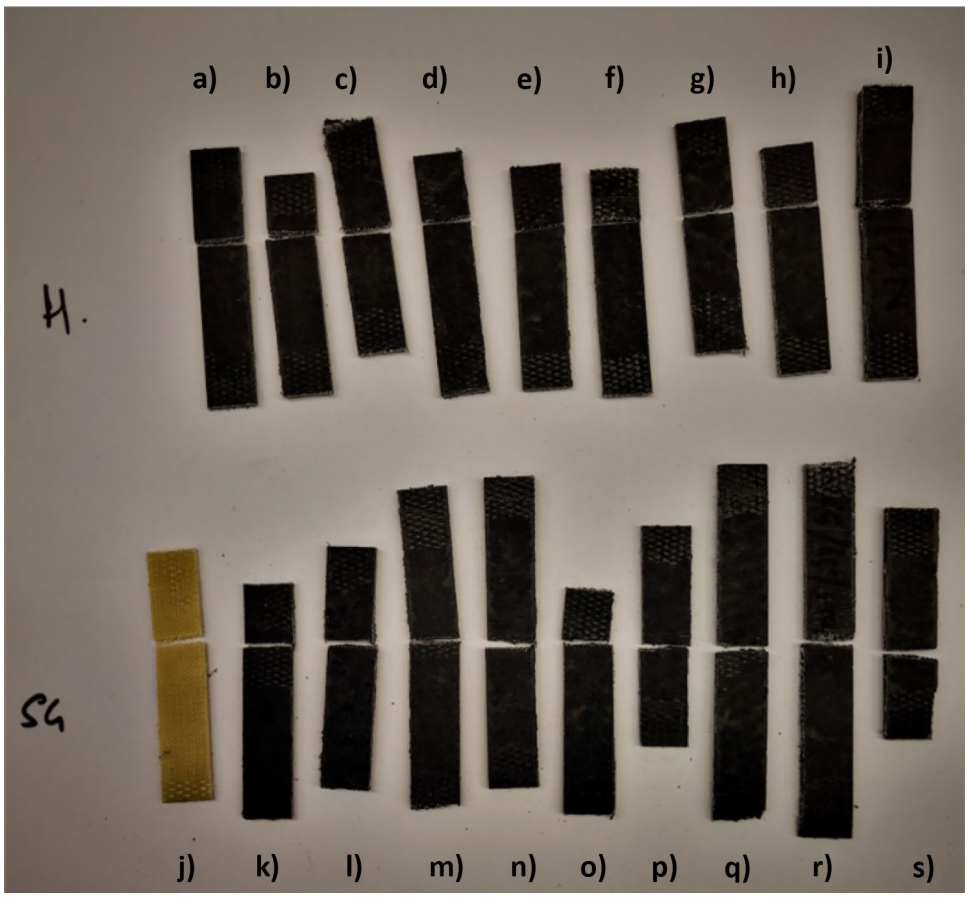

Fig. 13 Fractured samples from tensile test showing hemp biocarbon-filled hemp fiber reinforced composites with the letter as coded in Table 1

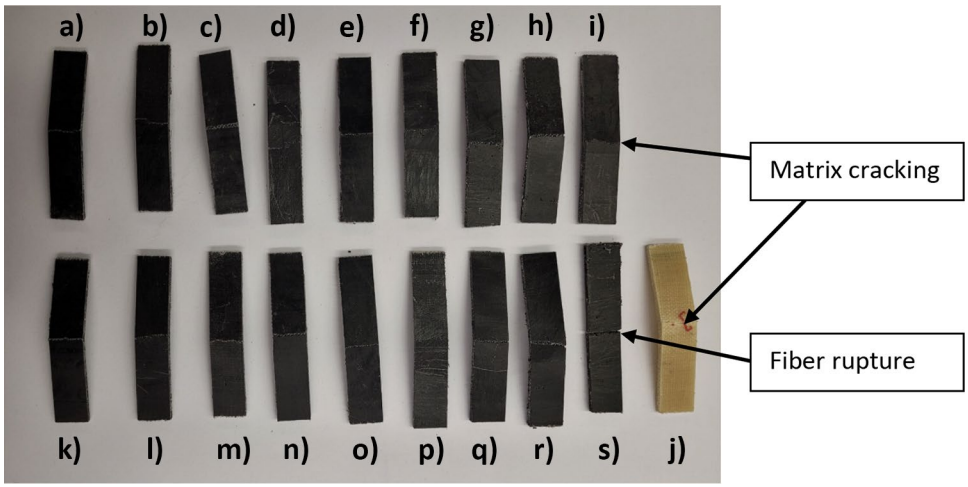

Fig. 14 Fractured samples from three-point bend showing hemp biocarbon-filled hemp fiber reinforced composites with the letter as coded in Table 1

In tensile loading, the failure occurred due to the breaking of both fibers and cracking of the polymer matrix. The first failure mode was the matrix cracking in the transverse direction, which resulted from the weaker nature of the polymeric matrix as compared to the longitudinally loaded hemp fibers. This caused a drop in the transverse tensile modulus of the composite material. The second failure mode was the lateral splitting of the fibers with further tensile load, followed by fiber fracture at higher loading levels.

In flexural loading, the failure occurred mainly due to polymer matrix failure, with delamination occurring near the fractured surface. This was followed by fiber breakage on further increment of the flexural loading. This failure mode can be attributed to the bending stresses acting on the composite material, which caused the polymer matrix to deform and eventually fail, leading to delamination and fiber breakage. The failure mechanism was due to the interplay between the tensile and flexural loading, the relative strengths of the fibers and matrix, and the propensity for delamination and fiber breakage.

Morphological study

The morphological study of the biocarbon samples from hemp stalk and switchgrass feedstock are presented in Figs. 15, 16, 17, 18, 19, 20. The images show the voids

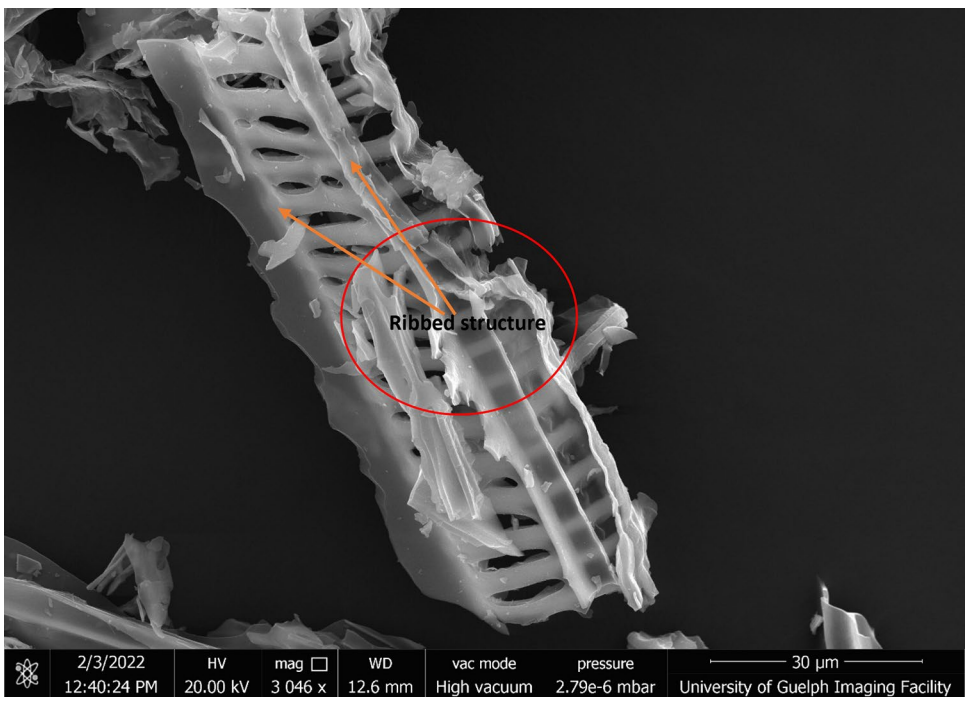

Fig. 15 The morphology of the hemp biocarbon obtained at 450 °C pyrolysis temperature

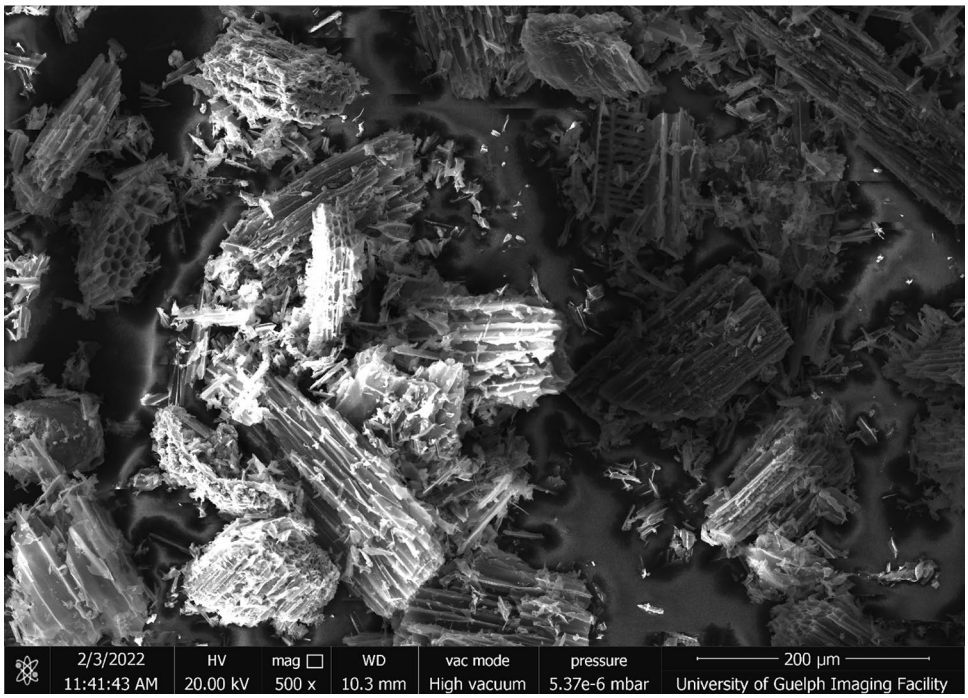

Fig. 16 The morphology of the hemp biocarbon obtained at 550 °C pyrolysis temperature

of the biocarbon samples responsible for its unique properties including low density and porosity. The inability of the resin to penetrate these pores would result in the poor filler-matrix interface resulting in weaker mechanical properties. The improved tensile strength of the biocomposite samples with biocarbon obtained at 650 °C is due to the formation of more mesopores and void rib like structure along with the micropores in the biocarbon surfaces during the removal of the volatile matter. These mesopores offer comparatively easier pathway for the polymer flow into the filler structure. As a result, the increased tensile strength was observed with the fillers obtained at 650 °C.

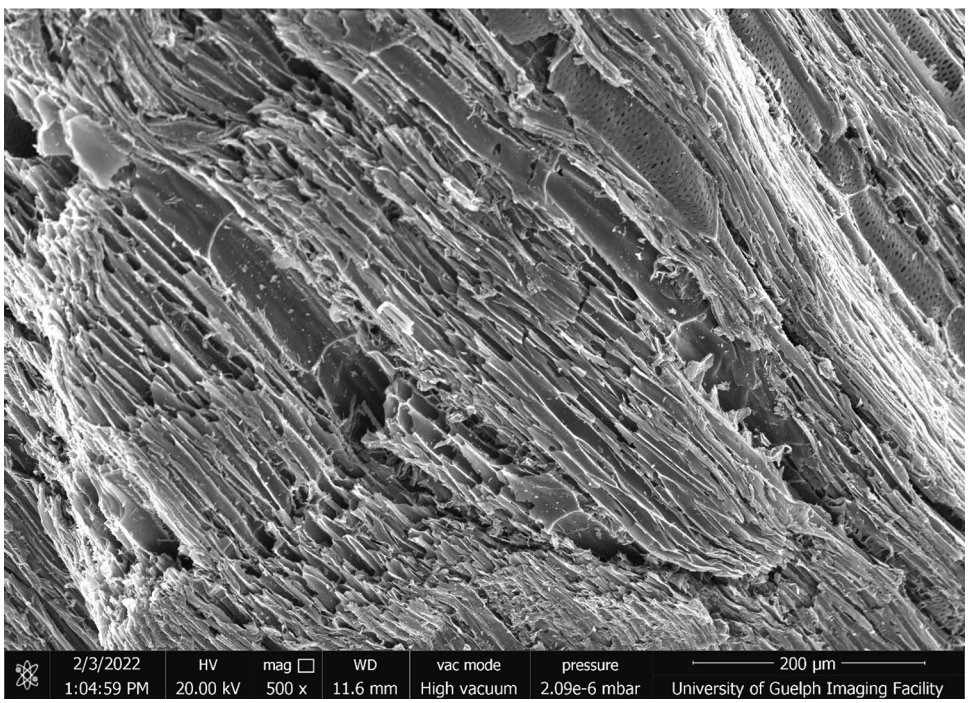

Fig. 17 The morphology of the hemp biocarbon obtained at 650 °C pyrolysis temperature

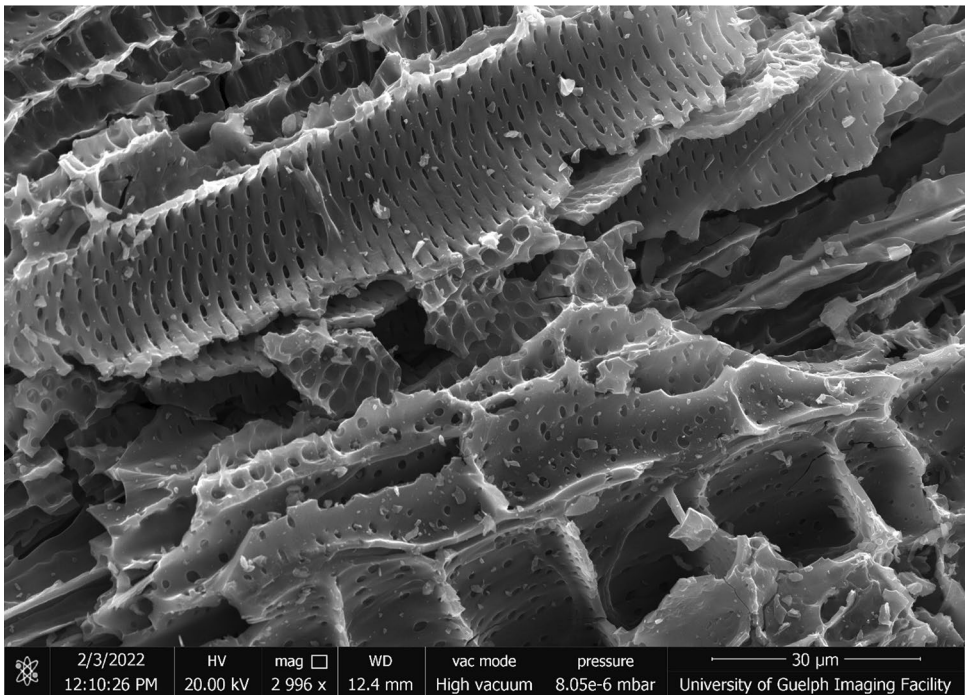

Fig. 18 The morphology of the switchgrass biocarbon obtained at 450 °C pyrolysis temperature

Due to the better tensile properties of the H65-50-10 and S65-50-10, competent mechanical behaviour of the HeR composites, and the poor performance of the H65-100-20 and S65-100-20, the morphological study of these samples has been presented in Fig. 21 to Fig. 25. The HeR composites showed better mechanical strength than the H65-100-20 because of the better fiber-polymer matrix adhesion relationship and utilization of the fiber pull-out to minimize

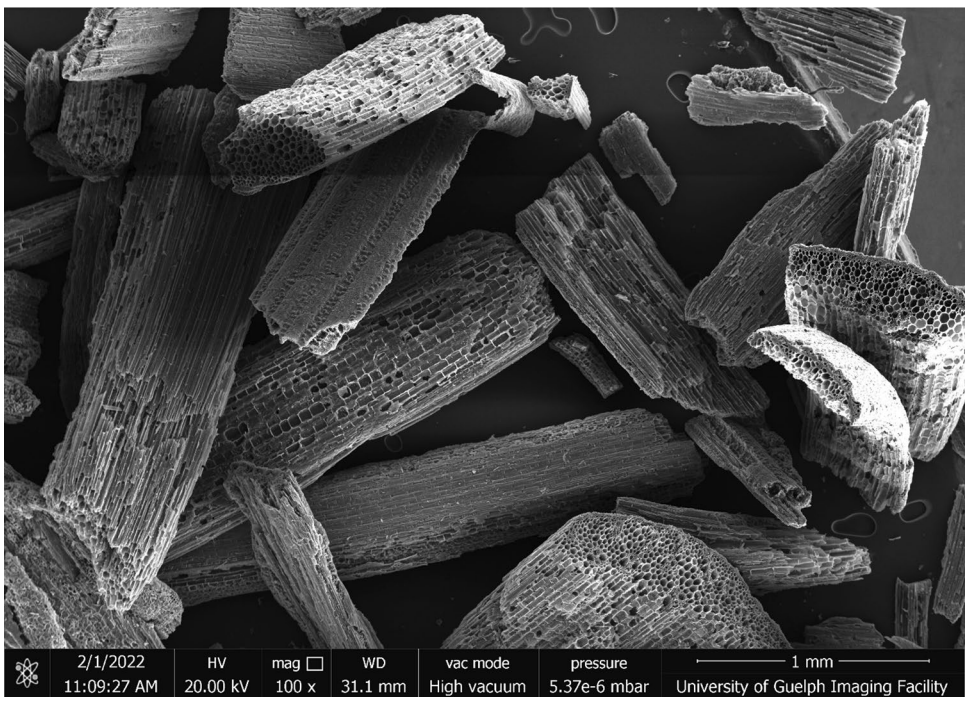

Fig. 19 The morphology of the switchgrass biocarbon obtained at 550 °C pyrolysis temperature

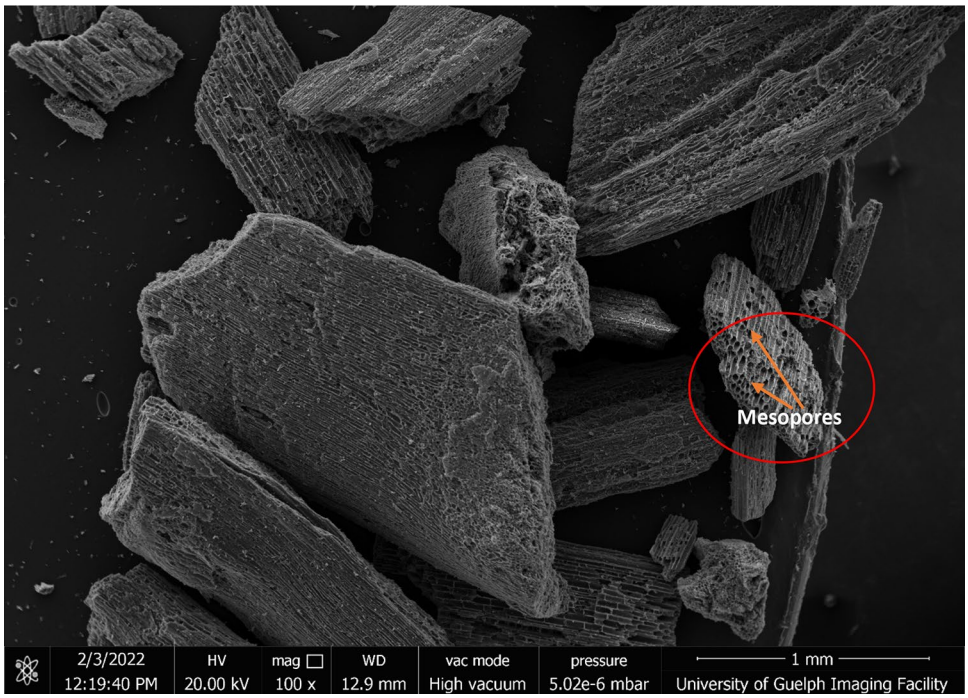

Fig. 20 The morphology of the switchgrass biocarbon obtained at 650 °C pyrolysis temperature

the fiber cracking as depicted in Fig. 21 to Fig. 25. Similarly, the better tensile strength of the H65-50-10 was due to the better adhesion between the polymer-filler matrix and the hemp fibers, the increased friction force between the matrix-fiber interface and the utilization of the fiber pull-out during the tensile loading (Figs. 22, 23, 24, 25).

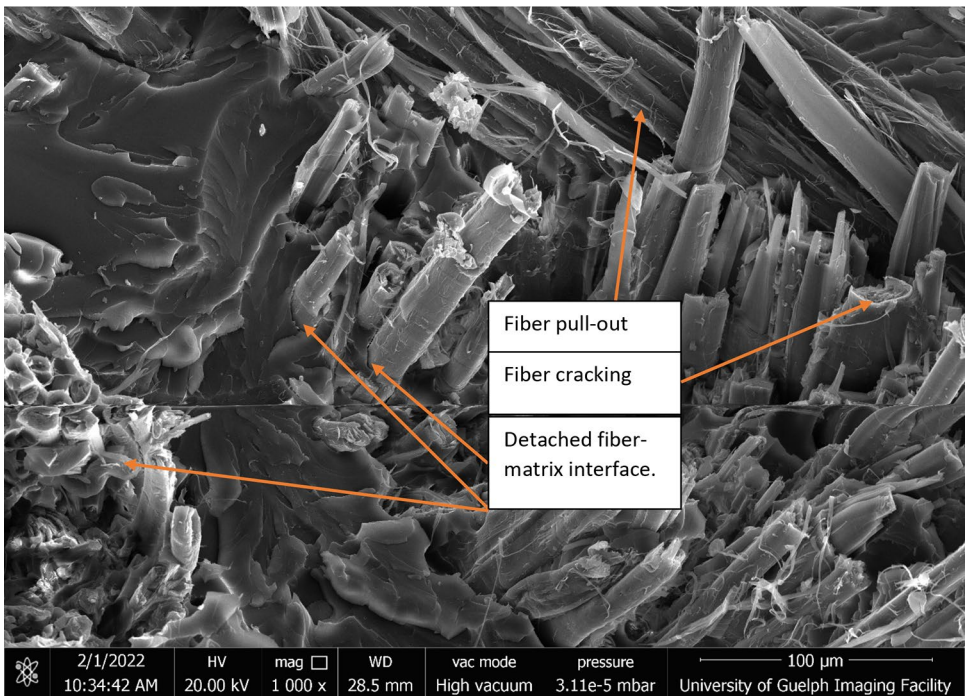

Fig. 21 FE-SEM images from the tensile tested HeR sample

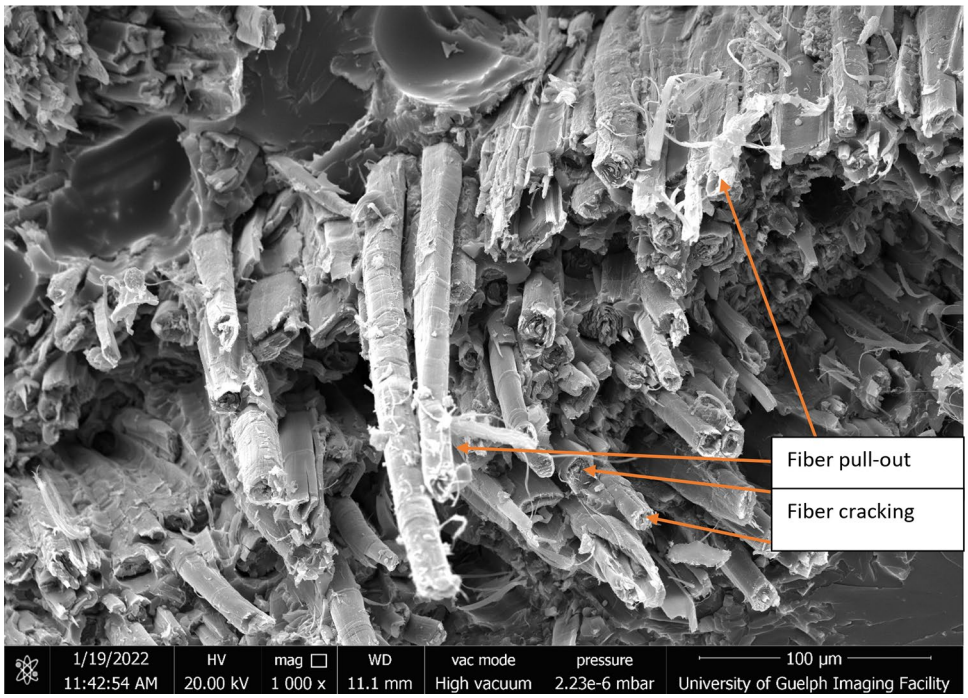

Fig. 22 FE-SEM images from the tensile tested H65-50-10 sample

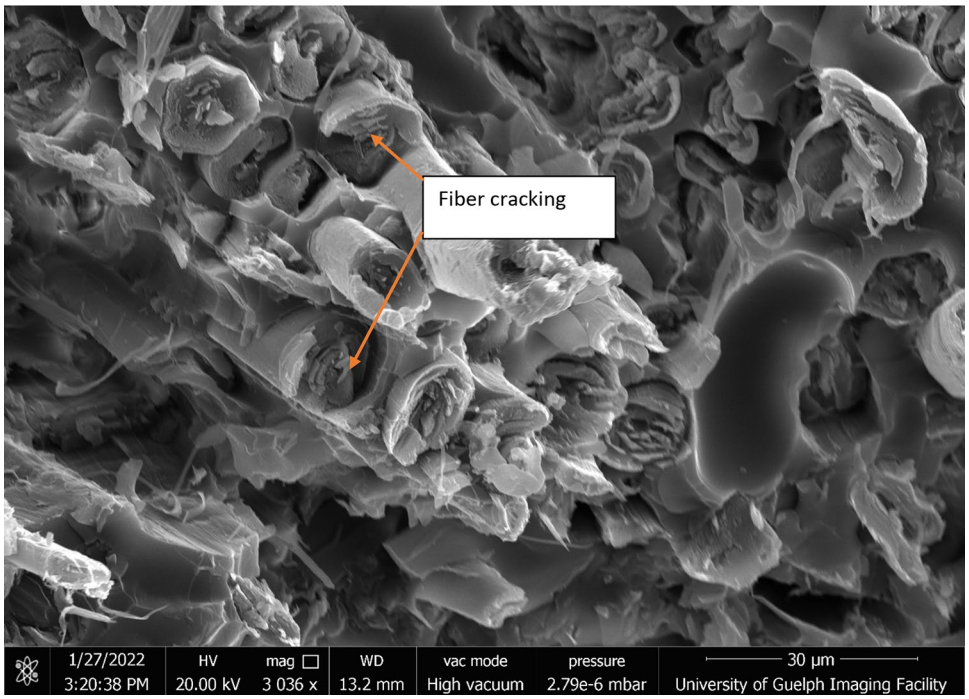

Fig. 23 FE-SEM images from the tensile tested S65-50-10 sample

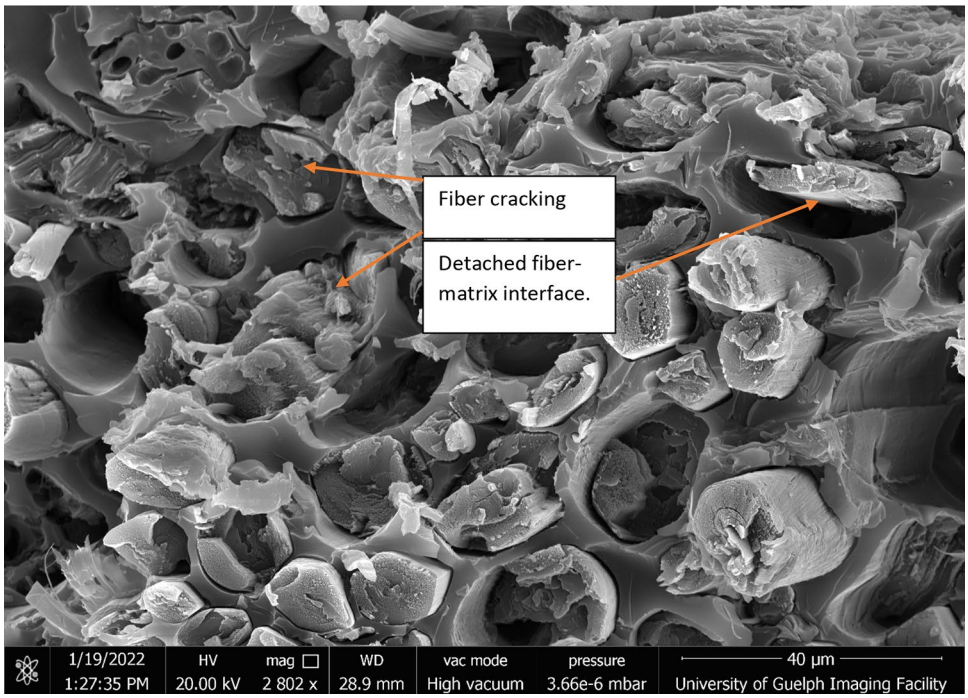

Fig. 24 SEM images from the tensile tested H65-100-20 sample

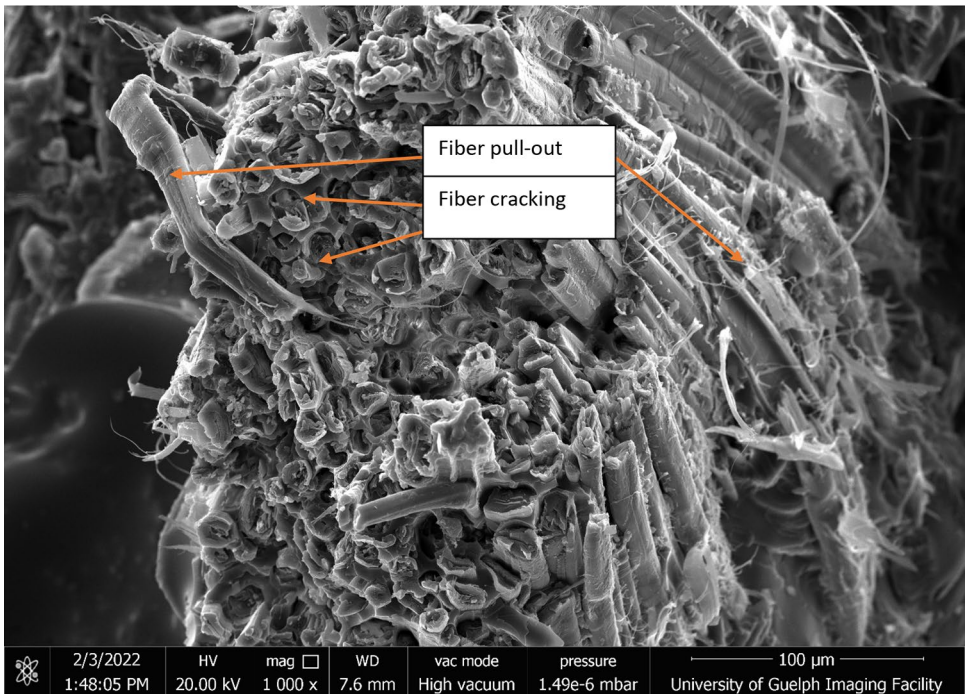

Fig. 25 SEM images from the tensile tested S65-100-20 sample

Conclusions

The biopolymer composites with and without hemp fiber reinforcement and with and without biocarbon fillers were fabricated. The maximum tensile strength was recorded as 840.75 MPa for the S65-50-10 followed by 817.02 MPa for the H65-50-10. The tensile strength of the hemp fiber reinforced unfilled polymer composite was determined to be 727.73 MPa. Tensile strength was indirectly proportional to the biocarbon concentration in the polymer composite. Irrespective of the biocarbon type, the tensile strength of the composite samples with 20% filler loading and 100 microns particle size biocarbon fillers obtained at 650 °C showed the weakest. The tensile strength at this condition was found to be 646.13 MPa and 553.64 MPa for hemp biocarbon and switchgrass biocarbon filled hemp fiber-reinforced composites, respectively. Tensile strength initially increased when the fillers' particle size was increased from 50 µm to 75 µm, and then decreased on further increasing the particle size to 100. The energy at tensile rupture was found to increase by increasing the fillers' particle size. The filler loading decreases the energy at break of the composite samples. The impact energy of the hemp fiber-reinforced unfilled polymer composites showed a value of 8.09 ± 2.22 J/m (as per the ASTM standard) and 630.31 J/m2 (as per the ISO standard). The biocarbon in the composite samples promotes earlier material failure during the impact loading). The impact strength of the composite samples decreased by almost 63% when filler loading was increased by 100% from 10 wt.% to 20 wt.%. The composites' hardness significantly increases with the increase in filler loading. The calculated specific tensile strength of values above 650 MPa/ (g.cc) of the optimized composite samples proves to be the most superior one among all plant fiber reinforced thermosetting composites and these hemp fiber-reinforced composites can replace the glassfiber reinforced composites in the tensile and flexural loading applications.

Acknowledgments The authors would like to offer a sincere gratitude towards the Utopia Hemp Company, Ontario, Canada and OBPC Farmers, Ontario, Canada for providing the biomass feedstock to conduct this research.

Author contributions Conceptualization - Raj Kumar Dahal; Methodology - Raj Kumar Dahal; Validation - Bishnu Acharya, Animesh Dutta; Formal analysis - Raj Kumar Dahal; Investigation - Raj Kumar Dahal; Resources - Bishnu Acharya, Animesh Dutta; Data curation – Raj Kumar Dahal, Bishnu Acharya; Writing—original draft - Raj Kumar Dahal; Writing—review and editing - Raj Kumar Dahal; Supervision - Bishnu Acharya, Animesh Dutta; Project Administration - Animesh Dutta; Funding acquisition - Animesh Dutta, Software – Raj Kumar Dahal, Bishnu Acharya, Animesh Dutta. All authors have read and agreed to the final version of the manuscript.

Funding sources This work was supported by the Natural Sciences and Engineering Research Council of Canada (NSERC), and Agriculture and Agri-Food Canada's AgriScience program Biomass Canada Cluster. Natural Sciences and Engineering Research Council of Canada,Discovery Grant,Animesh Dutta ,Agriculture and Agri-Food Canada,Biomass Canada Cluster,Animesh Dutta.

Data availability The authors declare that the data supporting the findings of this study are available within the paper and its Supplementary Information files. Should any raw data files be needed in another format they are available from the corresponding author upon reasonable request.

Declarations

Conflicts of interest There are no conflicts to declare.

References

1. Pickering KL, Efendy MGA, Le TM (2016) A review of recent developments in natural fibre composites and their mechanical performance. Compos Part A Appl Sci Manuf 83:98–112. https://doi.org/10.1016/j.compositesa.2015.08.038
2. Cao Y, Wu Y (2008) Evaluation of statistical strength of bamboo fiber and mechanical properties of fiber reinforced green composites. J Cent South Univ Technol 15:564–567. https://doi.org/10.1007/s11771-008-0422-z
3. Lee B-H, Kim H-J, Yu W-R (2009) Fabrication of long and discontinuous natural fiber reinforced polypropylene biocomposites and their mechanical properties. Fibers Polym 10:83–90. https://doi.org/10.1007/s12221-009-0083-z
4. Li X, Tabil LG, Panigrahi S (2007) Chemical Treatments of Natural Fiber for Use in Natural Fiber-Reinforced Composites: A Review. J Polym Environ 15:25–33. https://doi.org/10.1007/s10924-006-0042-3
5. Mehta G, Mohanty AK, Thayer K et al (2005) Novel Biocomposites Sheet Molding Compounds for Low Cost Housing Panel Applications. J Polym Environ 13:169–175. https://doi.org/10.1007/s10924-005-3211-x
6. Singha AS, Jyoti A (2013) Mechanical, morphological, and thermal properties of chemically treated pine needles reinforced thermosetting composites. J Appl Polym Sci 127:387–393. https://doi.org/10.1002/app.37636
7. Dev S, Aherwar A, Patnaik A (2019) Preliminary Evaluations on Development of Recycled Porcelain Reinforced LM-26/Al-Si10Cu3Mg1 Alloy for Piston Materials. Silicon 11:1557–1573. https://doi.org/10.1007/s12633-018-9979-9
8. Surappa MK (2003) Aluminium matrix composites: Challenges and opportunities. Sadhana 28:319–334. https://doi.org/10.1007/BF02717141
9. Sharma AK, Bhandari R, Aherwar A, Rimašauskienė R (2020) Matrix materials used in composites: A comprehensive study. Mater Today Proc 21:1559–1562. https://doi.org/10.1016/j.matpr.2019.11.086
10. Doddi PRV, Chanamala R, Dora SP (2020) Effect of fiber orientation on dynamic mechanical properties of PALF hybridized with basalt reinforced epoxy composites. Mater Res Express 7:015329. https://doi.org/10.1088/2053-1591/ab6771
11. Yong CK, Ching YC, Chuah CH, Liou N-S (2015) Effect of Fiber Orientation on Mechanical Properties of Kenaf-Reinforced

Polymer Composite. Bioresources 10:. https://doi.org/10.15376/biores.10.2.2597-2608
12. Alomayri T, Shaikh FUA, Low IM (2014) Effect of fabric orientation on mechanical properties of cotton fabric reinforced geopolymer composites. Mater Des 57:360–365. https://doi.org/10.1016/j.matdes.2014.01.036
13. Zhang H, Huang Y, Lin M, Yang Z (2022) Effects of fibre orientation on tensile properties of ultra high performance fibre reinforced concrete based on meso-scale Monte Carlo simulations. Compos Struct 287:115331. https://doi.org/10.1016/j.compstruct.2022.115331
14. Ramakrishnan T, Sathesh BM, Balasubramani S et al (2021) Effect of fiber orientation and mechanical properties of natural fiber reinforced polymer composites-A review. Paideuma J Res XIV:17–23
15. Cordin M, Bechtold T, Pham T (2018) Effect of fibre orientation on the mechanical properties of polypropylene–lyocell composites. Cellulose 25:7197–7210. https://doi.org/10.1007/s10570-018-2079-6
16. McCardle R, Bhattacharyya D, Fakirov S (2012) Effect of Reinforcement Orientation on the Mechanical Properties of Microfibrillar PP/PET and PET Single-Polymer Composites. Macromol Mater Eng 297:711–723. https://doi.org/10.1002/mame.201100220
17. Vinayagamoorthy R (2020) Effect of particle sizes on the mechanical behaviour of limestone-reinforced hybrid plastics. Polym Polym Compos 28:410–420. https://doi.org/10.1177/0967391119883163
18. Youssef Y, El-Sayed M (2016) Effect of Reinforcement Particle Size and Weight Fraction on the Mechanical Properties of SiC Particle Reinforced Al Metal Matrix Composites. Int Rev Mech Eng (IREME) 10:261. https://doi.org/10.15866/ireme.v10i4.9509
19. Yang Z, Fan J, Liu Y et al (2021) Effect of the Particle Size and Matrix Strength on Strengthening and Damage Process of the Particle Reinforced Metal Matrix Composites. Materials 14:675. https://doi.org/10.3390/ma14030675
20. Saba F, Zhang F, Liu S, Liu T (2019) Reinforcement size dependence of mechanical properties and strengthening mechanisms in diamond reinforced titanium metal matrix composites. Compos B Eng 167:7–19. https://doi.org/10.1016/j.compositesb.2018.12.014
21. Paknia A, Pramanik A, Dixit AR, Chattopadhyaya S (2016) Effect of Size, Content and Shape of Reinforcements on the Behavior of Metal Matrix Composites (MMCs) Under Tension. J Mater Eng Perform 25:4444–4459. https://doi.org/10.1007/s11665-016-2307-x
22. Gong Y, Niu P, Wang X et al (2012) Influence of processing temperatures on fiber dimensions and microstructure of polypropylene/hemp fiber composites. J Reinf Plast Compos 31:1282–1290. https://doi.org/10.1177/0731684412457887
23. Manaia JP, Manaia AT, Rodriges L (2019) Industrial Hemp Fibers: An Overview. Fibers 7:106. https://doi.org/10.3390/fib7120106
24. Ngaowthong C, Rungsardthong V, Siengchin S (2016) Polypropylene/hemp woody core fiber composites: Morphology, mechanical, thermal properties, and water absorption behaviors. Adv Mech Eng 8:168781401663831. https://doi.org/10.1177/1687814016638318
25. Sullins T, Pillay S, Komus A, Ning H (2017) Hemp fiber reinforced polypropylene composites: The effects of material treatments. Compos B Eng 114:15–22. https://doi.org/10.1016/j.compositesb.2017.02.001
26. Peltola H, Madsen B, Joffe R, Nättinen K (2011) Experimental Study of Fiber Length and Orientation in Injection Molded Natural Fiber/Starch Acetate Composites. Adv Mater Sci Eng 2011:1–7. https://doi.org/10.1155/2011/891940
27. Dupuis A, Pesce J-J, Ferreira P, Régnier G (2020) Fiber Orientation and Concentration in an Injection-Molded Ethylene-Propylene Copolymer Reinforced by Hemp. Polymers (Basel) 12:2771. https://doi.org/10.3390/polym12122771
28. Ferreira RTL, Ashcroft IA (2020) Optimal orientation of fibre composites for strength based on Hashin's criteria optimality conditions. Struct Multidiscip Optim 61:2155–2176. https://doi.org/10.1007/s00158-019-02462-w
29. Heitkamp T, Kuschmitz S, Girnth S et al (2022) Stress-adapted fiber orientation along the principal stress directions for continuous fiber-reinforced material extrusion. Prog Additive Manuf. https://doi.org/10.1007/s40964-022-00347-x
30. Sharba MJ, Leman Z, Sultan MTH (2019) Fatigue life prediction of textile/woven hybrid composites. In: Durability and Life Prediction in Biocomposites, Fibre-Reinforced Composites and Hybrid Composites. Elsevier, pp. 63–82
31. Hoa SV (2018) 2.1 Manufacturing of Composites – An Overview. In: Comprehensive Composite Materials II. Elsevier, pp. 1–23
32. Shahzad A (2013) A Study in Physical and Mechanical Properties of Hemp Fibres. Adv Mater Sci Eng 2013:1–9. https://doi.org/10.1155/2013/325085
33. Pickering KL, Beckermann GW, Alam SN, Foreman NJ (2007) Optimising industrial hemp fibre for composites. Compos Part A Appl Sci Manuf 38:461–468. https://doi.org/10.1016/j.compositesa.2006.02.020
34. Bambach MR (2017) Compression strength of natural fibre composite plates and sections of flax, jute and hemp. Thin-Walled Structures 119:103–113. https://doi.org/10.1016/j.tws.2017.05.034
35. Misnon I, Islam M, Epaarachchi J et al (2016) Fabric Parameter Effect on the Mechanical Properties of Woven Hemp Fabric Reinforced Composites as an Alternative to Wood Products. Adv Res Textile Eng 1
36. Hepworth DG, Hobson RN, Bruce DM, Farrent JW (2000) The use of unretted hemp fibre in composite manufacture. Compos Part A Appl Sci Manuf 31:1279–1283. https://doi.org/10.1016/S1359-835X(00)00098-1
37. Sature P, Mache A (2015) Mechanical Characterization and Water Absorption Studies on Jute/Hemp Reinforced Hybrid Composites. Am J Mater Sci 5:133–129. https://doi.org/10.5923/c.materials.201502.27
38. Liu M, Meyer AS, Fernando D et al (2016) Effect of pectin and hemicellulose removal from hemp fibres on the mechanical properties of unidirectional hemp/epoxy composites. Compos Part A Appl Sci Manuf 90:724–735. https://doi.org/10.1016/j.compositesa.2016.08.037
39. Dhakal H, Zhang Z, Richardson M (2007) Effect of water absorption on the mechanical properties of hemp fibre reinforced unsaturated polyester composites. Compos Sci Technol 67:1674–1683. https://doi.org/10.1016/j.compscitech.2006.06.019
40. Chandramohan D, Presin Kumar AJ (2017) Experimental data on the properties of natural fiber particle reinforced polymer composite material. Data Brief 13:460–468. https://doi.org/10.1016/j.dib.2017.06.020
41. Nan N, DeVallance DB, Xie X, Wang J (2016) The effect of biocarbon addition on the electrical, mechanical, and thermal properties of polyvinyl alcohol/biochar composites. J Compos Mater 50:1161–1168. https://doi.org/10.1177/0021998315589770
42. Zouari M, Devallance DB, Marrot L (2022) Effect of Biochar Addition on Mechanical Properties, Thermal Stability, and Water Resistance of Hemp-Polylactic Acid (PLA) Composites. Materials 15:2271. https://doi.org/10.3390/ma15062271
43. Zheljazkov VD, Maggi F (2021) Valorization of CBD-hemp through distillation to provide essential oil and improved cannabinoids profile. Sci Rep 11:19890. https://doi.org/10.1038/s41598-021-99335-4
44. Knezevic F, Nikolai A, Marchart R et al (2021) Residues of herbal hemp leaf teas – How much of the cannabinoids remain? Food Control 127:108146. https://doi.org/10.1016/j.foodcont.2021.108146
45. Burton RA, Andres M, Cole M et al (2022) Industrial hemp seed: from the field to value-added food ingredients. J Cannabis Res 4:45. https://doi.org/10.1186/s42238-022-00156-7

46. Matthäus B, Brühl L (2008) Virgin hemp seed oil: An interesting niche product. Eur J Lipid Sci Technol 110:655–661. https://doi.org/10.1002/ejlt.200700311
47. Leizer C, Ribnicky D, Poulev A et al (2000) The Composition of Hemp Seed Oil and Its Potential as an Important Source of Nutrition. J Nutraceuticals, Funct Med Foods 2:35–53. https://doi.org/10.1300/J133v02n04_04
48. Muangmeesri S, Li N, Georgouvelas D et al (2021) Holistic Valorization of Hemp through Reductive Catalytic Fractionation. ACS Sustain Chem Eng 9:17207–17213. https://doi.org/10.1021/acssuschemeng.1c06607
49. Francis JT, Hitchcock AP (1992) Inner-shell spectroscopy of p-benzoquinone, hydroquinone, and phenol: distinguishing quinoid and benzenoid structures. J Phys Chem 96:6598–6610. https://doi.org/10.1021/j100195a018
50. Singh B, Fang Y, Cowie BCC, Thomsen L (2014) NEXAFS and XPS characterisation of carbon functional groups of fresh and aged biochars. Org Geochem 77:1–10. https://doi.org/10.1016/j.orggeochem.2014.09.006
51. Kaznacheyev K, Osanna A, Jacobsen C et al (2002) Innershell Absorption Spectroscopy of Amino Acids. J Phys Chem A 106:3153–3168. https://doi.org/10.1021/jp013385w
52. Schäfer T, Buckau G, Artinger R et al (2005) Origin and mobility of fulvic acids in the Gorleben aquifer system: implications from isotopic data and carbon/sulfur XANES. Org Geochem 36:567–582. https://doi.org/10.1016/j.orggeochem.2004.10.011
53. Schumacher M, Christl I, Scheinost AC et al (2005) Chemical Heterogeneity of Organic Soil Colloids Investigated by Scanning Transmission X-ray Microscopy and C-1s NEXAFS Microspectroscopy. Environ Sci Technol 39:9094–9100. https://doi.org/10.1021/es050099f
54. Solomon D, Lehmann J, Kinyangi J et al (2005) Carbon K-Edge NEXAFS and FTIR-ATR Spectroscopic Investigation of Organic Carbon Speciation in Soils. Soil Sci Soc Am J 69:107–119. https://doi.org/10.2136/sssaj2005.0107dup
55. Heymann K, Lehmann J, Solomon D et al (2011) C 1s K-edge near edge X-ray absorption fine structure (NEXAFS) spectroscopy for characterizing functional group chemistry of black carbon. Org Geochem 42:1055–1064. https://doi.org/10.1016/j.orggeochem.2011.06.021
56. Kleber M, Nico PS, Plante A et al (2011) Old and stable soil organic matter is not necessarily chemically recalcitrant: implications for modeling concepts and temperature sensitivity. Glob Chang Biol 17:1097–1107. https://doi.org/10.1111/j.1365-2486.2010.02278.x
57. Keiluweit M, Bougoure JJ, Zeglin LH et al (2012) Nano-scale investigation of the association of microbial nitrogen residues with iron (hydr)oxides in a forest soil O-horizon. Geochim Cosmochim Acta 95:213–226. https://doi.org/10.1016/j.gca.2012.07.001
58. Yang G, Heo Y-J, Park S-J (2019) Effect of Morphology of Calcium Carbonate on Toughness Behavior and Thermal Stability of Epoxy-Based Composites. Processes 7:178. https://doi.org/10.3390/pr7040178
59. Głogowska K, Majewski L (2017) The effect of selected natural fillers on the mechanical properties of low-density polyethylene. Technical Transactions, Mechanics 155–166. https://doi.org/10.4467/2353737XCT.17.181.7289
60. Paukszta D, Szostak M, Rogacz M (2014) Mechanical properties of polypropylene copolymers composites filled with rapeseed straw. Polimery 59:165–169. https://doi.org/10.14314/polimery.2014.165
61. Morreale M, Scaffaro R, Maio A, La Mantia FP (2008) Effect of adding wood flour to the physical properties of a biodegradable polymer. Compos Part A Appl Sci Manuf 39:503–513. https://doi.org/10.1016/j.compositesa.2007.12.002
62. Sahoo S, Misra M, Mohanty AK (2013) Effect of compatibilizer and fillers on the properties of injection molded lignin-based hybrid green composites. J Appl Polym Sci 127:4110–4121. https://doi.org/10.1002/app.37667
63. Dányádi L, Móczó J, Pukánszky B (2010) Effect of various surface modifications of wood flour on the properties of PP/wood composites. Compos Part A Appl Sci Manuf 41:199–206. https://doi.org/10.1016/j.compositesa.2009.10.008
64. Ahmad J, Burduhos-Nergis DD, Arbili MM et al (2022) A Review on Failure Modes and Cracking Behaviors of Polypropylene Fibers Reinforced Concrete. Buildings 12:1951. https://doi.org/10.3390/buildings12111951
65. Andiç-Çakir Ö, Sarikanat M, Tüfekçi HB et al (2014) Physical and mechanical properties of randomly oriented coir fiber–cementitious composites. Compos B Eng 61:49–54. https://doi.org/10.1016/j.compositesb.2014.01.029
66. Giorcelli M, Khan A, Pugno NM et al (2019) Biochar as a cheap and environmental friendly filler able to improve polymer mechanical properties. Biomass Bioenergy 120:219–223. https://doi.org/10.1016/j.biombioe.2018.11.036
67. Giurgiutiu V (2016) Damage and Failure of Aerospace Composites. In: Structural Health Monitoring of Aerospace Composites. Elsevier, pp. 125–175